



Erasmus+



## Master in Computational Colour and Spectral Imaging (COSI)



NTNU  
Norwegian University of  
Science and Technology

### Visual Display Calibration

Master Thesis Report

Presented by

Maria-Jose Rueda Montes

and defended at the

Norwegian University of Science and Technology

September 2022

Academic Supervisor(s): Peter Nussbaum and Seyed Ali Amirshahi  
Jury Committee:

1. Eva María Valero Benito, Universidad de Granada
2. Philippe Colantoni, Université Jean Monnet

Submission of the thesis: 10<sup>st</sup> August 2022  
Day of the oral defense: 2<sup>nd</sup> September 2022

# Abstract

Color mismatch between display devices is a relevant issue in color-critical applications. Here we propose a display calibration technique based on visual judgments that do not require a measurement device. Our calibration method is divided into two main stages, the psychophysical data collection, and the computation of the matrix-based transformation that will be applied per pixel to perform the color calibration. To collect the data, we designed a user-friendly graphical user interface (GUI) that allows the observer to define the display characteristics using their own chosen hues. The selected color points become the foundation for the personalized calibration file. This file stores the color coordinates of the observer selections, the hue planes, the neutral grey, and the signal-to-light-intensity function. We leverage the data from the calibration file to create three different matrix-based transformations. These transformations are then tested on two separate pairs of displays, using two distinct sets of hue combinations. This allows us to evaluate the effectiveness of the transformations across different display technologies and color variations. Our results indicate that the proposed transformation effectively preserves the greyscale across displays, especially when dealing with significant color differences. This suggests its usefulness in maintaining accurate neutral tones. Furthermore, when testing our new set of binary hues compared with the traditional set of unique hues, we obtained similar calibration results, suggesting the potential benefit of including the binary hue in the calibration method. Ideally, we should choose hues with the least variation in user perception (inter-observer variability). This will lead to more accurate color mapping, resulting in a faster and more reliable calibration process.

# Acknowledgment

First, I would like to thank my advisors, Peter Nussbaum and Seyed Ali Amirshahi, for guiding the project and answering any questions I had.

I must express my gratitude to the 13 observers who participated in the psychophysical experiments of this project.

Finally, I want to acknowledge the Norwegian University of Science and Technology, which provides the installations and devices necessary to conduct the project experiments.

# Contents

<b>1</b>	<b>Introduction</b>	<b>2</b>
1.1	Motivation & Objective . . . . .	2
1.2	Approach . . . . .	3
1.3	Novelty . . . . .	3
1.4	Structure . . . . .	4
<b>2</b>	<b>Theoretical Background</b>	<b>6</b>
2.1	Color management . . . . .	6
2.1.1	Color management components . . . . .	6
2.1.2	Three Cs of color management . . . . .	7
2.2	Color Models . . . . .	9
2.2.1	Device-Independent Color Models . . . . .	9
2.2.2	Device-Dependent Color Models . . . . .	13
2.2.3	Web colors and Okhsv . . . . .	15
2.3	Display Calibration . . . . .	16
2.3.1	Calibration parameters . . . . .	17
2.3.2	Calibration accuracy limitations . . . . .	19
2.3.3	Display Characterization . . . . .	20
2.4	Review on visual display calibration . . . . .	22
<b>3</b>	<b>Data collection</b>	<b>23</b>
3.1	Experimental Interface design (Stimuli) . . . . .	23
3.2	Experimental Methodology . . . . .	25
3.3	Neutral background stage . . . . .	26
3.4	Hue selections stage . . . . .	29
3.4.1	Binary hues . . . . .	31
3.4.2	Color spaces . . . . .	32
<b>4</b>	<b>Calibration Method</b>	<b>34</b>
4.1	Display Calibration Process . . . . .	34
4.2	Display Calibration Methodology . . . . .	35
4.2.1	Hues combinations . . . . .	37
4.2.2	Designed profiles . . . . .	38
4.2.3	Conversions . . . . .	39
4.3	Display Characterization . . . . .	40
4.4	Display Profile . . . . .	41

## CONTENTS

4.5	Matrix-Based transformations . . . . .	42
4.5.1	Point to Point Transformation . . . . .	43
4.5.2	Point to Plane Transformation . . . . .	44
4.5.3	White Preservation Transformation . . . . .	45
4.6	Evaluation of Calibration . . . . .	46
<b>5</b>	<b>Results and Discussion</b>	<b>47</b>
5.1	From Display 1 to Display 2 . . . . .	47
5.1.1	Color differences per ColorChecker patch . . . . .	47
5.1.2	Color differences per Observer . . . . .	48
5.2	From Display 1 to Display 3 . . . . .	49
5.2.1	Color differences per ColorChecker patch . . . . .	51
5.2.2	Color differences per Observer . . . . .	51
5.3	Hue combinations . . . . .	53
<b>6</b>	<b>Conclusions</b>	<b>56</b>
6.1	Summary . . . . .	56
6.2	Future Work . . . . .	57
<b>Bibliography</b>		<b>58</b>
<b>List of Figures</b>		<b>63</b>
<b>List of Tables</b>		<b>65</b>

# 1 | Introduction

## 1.1 Motivation & Objective

When an image is viewed on a display unit, its color appearance depends on several factors, such as the physical properties of the display, and the viewing environment. Thus, when the same image is displayed on two different displays, they are likely not to match.

In the age of online communication, the color accuracy reproduction between display devices is becoming increasingly important. On top of that, because of the COVID-19 pandemic, activities that could previously be carried out face-to-face in a dedicated physical location, such as psychophysical experiments or color inspection of commercial products, have had to move online. In most experiments, especially those related to color choices, the displayed color appearance is a key factor (Lago, 2021). Another example of a problematic situation is when selling a product on the web. For example, in the textile sector, the color of the product is an essential attribute which influence the purchase decision (Wuerger, 2008); in an ideal situation, the appearance of the item and the one shown on display would match. More recently, the emergence of Virtual Reality (VR) technologies have emphasized the importance of accurately communicating color. Examples include the immersive clothing virtual wear (Niu, 2020), VR for clinical education (Mehrfard et al., 2021), or virtual Museums (Sik Lányi and Schanda, 2011), in which color appearance is a crucial element.

Typically, the color mismatch between displays is addressed using common color spaces, such as sRGB, the standard color space on the web. However, if the target display is not adjusted to the sRGB specifications, the color appearance will still be different than expected. In order to reproduce the desired color behavior, measuring devices are usually used, which are expensive and not available to every user. On the other hand, hardware-independent softwares also exists, which are based on human visual responses, but most of them focus on parameters such as contrast or luminance, but not on color. There is not much research about hardware independent colorimetric calibration, and the available methods have not been extensively tested.

Considering the problematic color mismatch in a wide variety of applications, there is an increasing need to provide solutions. Therefore, this project aims to improve the preservation of color appearance across display devices by using human judgments rather than an external measurement instrument.

## 1.2 Approach

Two visual judgment-based colorimetric calibration approaches were found in the literature. (Mulligan, 2009) which compute the calibration method by matching a display color with a physical reference (printed dollar with known colorimetric coordinates). In another work, Karatzas and Wuerger (2007) use the concept of unique hues to perform visual judgments that will define the color properties of the display and thus perform the calibration. For this project, the method proposed by Karatzas and Wuerger (2007) was selected as a reference, which is purely based on visual judgments.

The unique hues concept was first mentioned by Aubert and Mach in 1865 as “principal colors” and “basic color sensations” (Bao et al., 2020). Later, in 1905, Ewald Hering (Hering, 1964), described color appearance mechanism by using two pair of hues, red-green and yellow-blue. There is no color that can simultaneously contain one of the pairs of hues at the same time. For example, a red hue can never appear greenish. This assumption is important in color vision, and the four elementary colors (red, green, blue, and yellow) derived from this theory are known as unique hues. Color calibration using unique hues is based on the concept that unique hues are approximately constant across culture, gender, age, race, etc., and individual differences in color sensitivity do not affect the unique hue judgments. Therefore, observers are supposed to make similar unique hue judgments.

The visual calibration workflow starts by performing psychophysical experiments where a number of visual judgments are collected from the observers using a graphical user interface. These judgments are about selecting unique hues. The experiments are divided into two main stages: first, Neutral background, and second, Hue selections. From the neutral gray judgments, as the name suggests, the achromatic gray that serves as a background during the hue selections stage is obtained. Next, in the hue selection stage, hue judgments are collected which are used to construct the specific device profile (calibration file) that characterizes the color properties of the display. The profile from two display devices are used to compute the transformation method that converts its pixel values to match each other.

## 1.3 Novelty

This study has four main contributions. The first contribution is the development of an open-source graphic user interface to collect unique and binary hues judgments and to calculate the neutral background for a specific device. This software is

coded in JavaScript so it can be run online (Rueda, 2022).

The second contribution is the implementation of additional features in the data collection method compared to the one described by Karatzas and Wuergler (2007). We included a slight annulus rotation which its aim is to prevent successive contrast. An additional rotation and randomization were also implemented to prevent biased responses (section 3.1). It is also provided a formula to calculate the correct displayed hue angles during the neutral background stage (section 3.1). Last, we implemented a new color space (Okhsv), replacing the traditional HSV.

The third contribution is the test of three matrices to calibrate a display device. We proposed two of them (subsection 4.5.1 and subsection 4.5.3). These transformations were applied to two pairs of simulated displays. To this end, we designed three device profiles, which were applied to the same display and thus are simulated independent displays.

The fourth contribution is the inclusion of a binary hue to perform experiments and compute the calibration method (section 3.4). Then, we tested the transformation matrices in two sets of hues: red, green, blue, and yellow (unique hues); and red, green, blue, and orange.

## 1.4 Structure

In Chapter 2, the theoretical background is provided; Section 2.1 includes key concepts of color management to understand the process of calibration; Section 2.2 describes the most frequent color models used on displays and gives a view of the importance of color spaces in the color communication process; Section 2.3 is focused on calibration applied to displays; finally, Section 2.4 provides a review of previous works in the field of visual calibration.

In Chapter 3, the designed graphical user interface and the conducted experiments are presented in detail. There are two main stages, the neutral background stage and hue selections stage; Section 3.1 starts by describing the GUI common features between different stages; Section 3.2 explains the experimental procedure used to conduct the experiments. The workflow is visualized; Section 3.3 details the neutral background stage; Section 3.4 is dedicated to the hue selection stage. This section also explains why a binary hue and the Okhsv color space are implemented.

In Chapter 4, the steps after the data collection from the previous chapter are described. The data is employed to perform the calibration method; Section 4.1 overviews the calibration process; Section 4.2 schematize the calibration process performed. It describes the calibration workflow; Section 4.3 shows the non-device characterization alternatives for the visual calibration method; Section 4.4 explains the device profile creation and its content; Section 4.5 describes the matrices

calculations; Section 4.6 indicate the evaluation method used in the evaluation of the calibration performance.

In Chapter 5, the results and discussion are presented; Section 5.1 shows the transformation performance from Display 1 to Display 2; Section 5.2 shows the transformation results from Display 1 to Display 3; Section 5.3 discuss the binary hue implementation.

In Chapter 6, conclusions and future work are presented.

## 2 | Theoretical Background

This chapter explains a helpful theoretical introduction to understanding the later chapters. It includes key definitions and terminology to contextualize the process of display calibration. The last section of this chapter reviews previous work on remote calibration. Additionally, it is important to note that the explained concepts are display oriented. Other devices, such as printers, are mostly not being considered.

### 2.1 Color management

In color imaging, most devices behave differently despite receiving the same input values. For example, the same pixel values (RGB) in different display devices will produce dissimilar color appearance responses. In order to match them, it is necessary to adjust the instructions given to the pixels. These adjustments can be made by applying Color Management (Sharma, 2018). Color management is defined as the process that enables the correct communication of the color content data and the necessary color conversions to produce the desired response (Consortium, 2020).

#### 2.1.1 Color management components

Today, color is managed through Color Management Systems (CMS). In a color imaging device, CMS has the task of interpreting the relationship between the input signal values and the perceived color outputs, and performing the appropriate transformations that keep a consistent color appearance between devices. To reduce the number of device-to-device transformations, the input signals are converted into a standard intermediary space, called Profile Connection Space (PCS) (Fraser et al., 2002).

The International Color Consortium (ICC)<sup>1</sup> has defined a PCS that serves as a common color space between devices (Sharma and Bala, 2017). To link each device to the PCS, the device profiles are employed. Profiles describe the relationship between the device signals and the actual color appearance. Consequently, the

---

<sup>1</sup>ICC defines international standards in color management. The explained ICC components intent to give an overview of the color management structure. Note that some of the notations are not mentioned again. More detailed information about the ICC format is able in (Consortium, 2022b).

ICC profiles are standard device profiles that contain the required transformations between the device data and the PCS (Consortium et al., 2004). The engine responsible for interpreting the device ICC profiles, and performing the calculations to convert the color data to and from the reference color space, is referred to as Color Management Module (CMM).

Due to the physical limitations of a device, even after a perfect color management process, the device's output images may not be able to match. The range of colors that can produce a device is called color gamut. Displays use different imaging technologies, such as CRT, LCD, or OLED, resulting in mismatched color gamuts (Sharma, 2018). For handling out-of-gamut colors, color management utilizes rendering intents. ICC specifies four rendering intents options: perceptual, saturation, relative colorimetric, and absolute colorimetric. Perceptual and saturation renderings perform gamut compression by desaturating the source colors. Whereas relative and absolute colorimetric compute gamut clipping, which cuts out the out-of-gamut colors (Fraser et al., 2002).

## 2.1.2 Three Cs of color management

Practical color management processes involves three main operations: calibration, characterization and conversion (three Cs) (Sharma, 2018). These three operations work together to enable a correct color reproduction as shown in Figure 2.1.

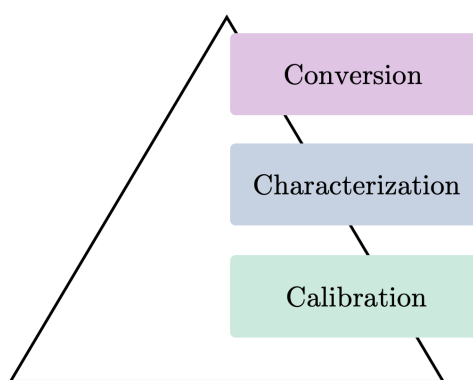


**Figure 2.1:** Hierarchical steps that define the color management process.  
(Illustration inspired by Sharma (2018).)

Calibration maintains the device with a fixed characteristic color response, aiming for a repeatable and reproducible color behavior. To this end, the calibration process is able to restore the device to a predefined state (Consortium et al., 2004). Additionally, when the intention is to achieve a specific color behavior, the

## Chapter 2 | THEORETICAL BACKGROUND

calibration process requires color measurements or visual judgments to compute the corrections that preserve the preferred characteristic (Sharma and Bala, 2017).

For a calibrated device, the characterization defines the color characteristics of that particular device, it relates device-dependent and device-independent color representations (section 2.2). The CMSs, during the characterisation process, create the profile that saves the device's behaviour (Consortium, 2008). There are two main directions of characterization (Figure 2.2). Forward characterization predicts the output of a calibrated device from a known input, while inverse characterization determines the input required to obtain the desired response (Sharma and Bala, 2017).

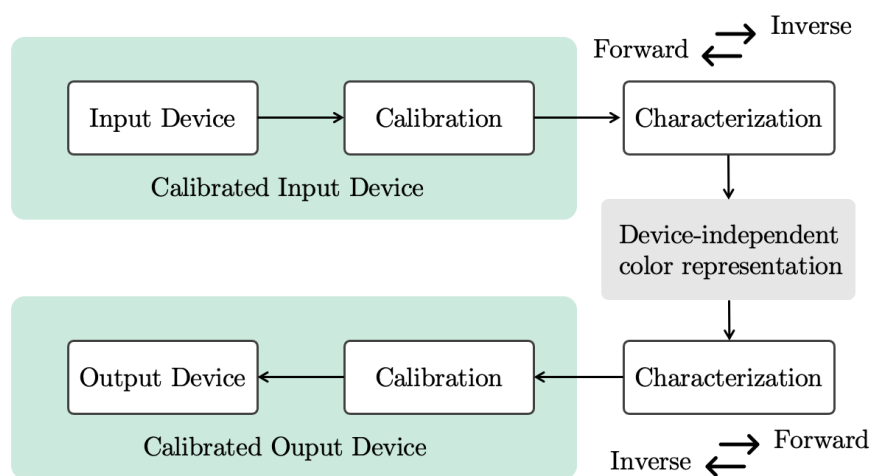


**Figure 2.2:** Calibration and characterization workflow in input and output devices. (Illustration inspired by Sharma and Bala (2017).)

Calibration and characterization are closely related. When a new calibration changes the color responses of a device, the characterization is no longer valid, and it has to be computed again. A calibrated device ensures the characterization is working properly (Sharma and Bala, 2017).

Conversion is the step where the data from one color space is transformed into another. In two different devices, it may define the mathematical calculations that relate both device color spaces (Johnson, 1996). Then, the profiles of each device are typically used in the color conversion phase (Sharma and Bala, 2017).

## 2.2 Color Models

Color models provide a consistent categorization of colors. To correctly follow the color management process, is essential to define the different forms of color representation.

Before computers existed, categorizing and describing colors was already a subject of study. From this search were originated the perceptual color models, such as Munsell Color System or the Natural Color System (NCS). The Munsell color system (Cochrane, 2014), one of the most widely known color-order systems, is a three-dimensional model that orders colors according to three attributes: hue, value, and chroma. Albert H.Munsell created the system in the 1890s to specify colors visually and numerically (Sharma, 2018). It is important to mention this color system not only because it is still popular in the industry, but also because it has served as inspiration in the creation of modern color spaces (Rhyne, 2017), such as CIELUV, CIELAB, HSV or Okhsv (Ottosson, 2021b).

New color models can be divided into two categories according to their fundamentals: based on additive color mixing or based on color matching functions. In an additive color-mixing model, a new color is generated by adding a set of wavelengths, for example, mixing three different light sources, as in the case of RGB pixels. Within this category are the RGB color spaces (Fraser et al., 2002). On the other hand, color spaces based on color matching functions originated from visual experiments conducted on humans. During the experiments, the observers had to match a colored reference stimulus using three RGB lights. The proportion of each RGB light used to obtain the match describes the tristimulus values, which are the basis of color models like CIE XYZ, CIELUV, or CIELAB (Rhyne, 2017).

### 2.2.1 Device-Independent Color Models

Device-independent color models aim to describe color in terms of human perception (Fraser et al., 2002). The Commission Internationale d'Eclairage (CIE), or in English—International Commission of Illumination, describes a series of standardized device-independent color models, such as CIE XYZ, CIELAB, or CIELUV. Besides, within the device-independent color models can also be included complete specifications of the RGB color space, which comprise sRGB, Adobe RGB, or ProPhoto RGB, among others (Rhyne, 2017).

### 2.2.1.1 CIE Color Specification

In 1931, CIE proposed the first model that mathematically describes color perception. This three-dimensional model was called CIE XYZ and is based on a standard set of color-matching functions. XYZ are known as tristimulus values, and they represent the required amount of primaries to match a stimulus. One of the first created two-dimensional projections from this space (where hue and saturation are distributed in a plane) is well-known as the CIE xy chromaticity diagram (Figure 2.3a) (Elliot et al., 2015). Even though tristimulus and chromaticity spaces are useful for concluding whether two stimuli appear to match, they are not considered color spaces. Proper color spaces are able to quantify the appearance of the stimulus, these include CIELAB, and CIELUV (Elliot et al., 2015).

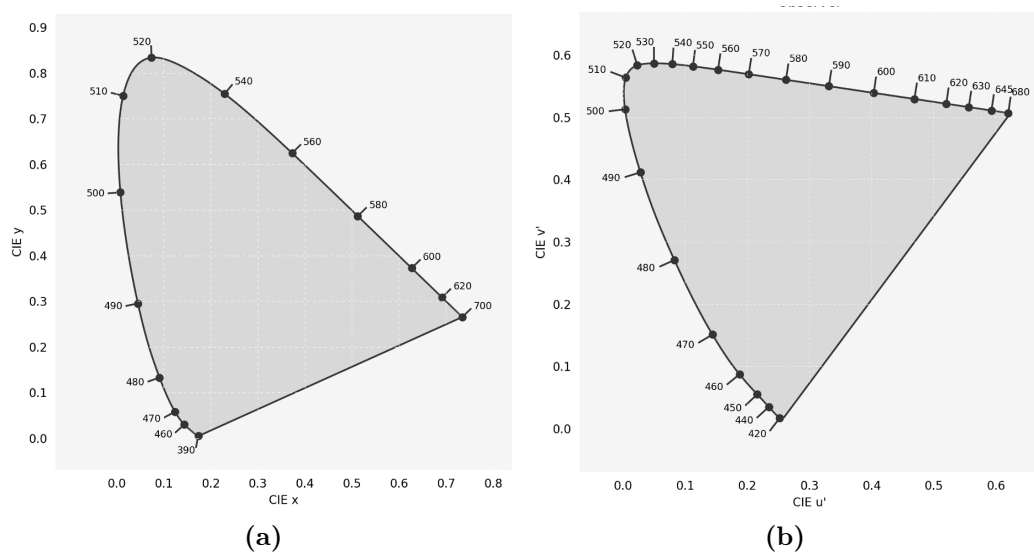


**Figure 2.3:** (a) CIE 1931 Chromaticity Diagram - CIE 1931 2° Standard Observer. (b) CIE 1976 Chromaticity Diagram - CIE 1931 2° Standard Observer

CIELAB and CIELUV are extensions of the CIE XYZ model that specify perceptual attributes of lightness, chroma, and hue. Their use was recommended by CIE in 1976 (Elliot et al., 2015). To modulate color appearance, both color spaces include visual system behavior features under determined viewing conditions. CIELAB intends to be a perceptual uniform color space able to describe the difference in terms of color between two stimuli. The three-dimensional axes of the CIELAB color space are based on the opponent process theory of color vision. A color stimulus is located in the CIELAB space using the  $L^*a^*b^*$  coordinates. The  $L^*$  axis is vertical and describes the lightness from 0, black, to 100, a diffuse white. The  $a^*$  and  $b^*$  axes are in a perpendicular plane to  $L^*$ . In this case, they describe

the chroma from 0 to 100, 100 being the value of a full chromatic stimulus. The  $a^*$  axis changes from red ( $+a$ ) to green ( $-a$ ), and the  $b^*$  axis from yellow ( $+b$ ) to blue ( $-b$ ) (Sharma, 2018). When the CIELAB color space is represented in cylindrical coordinates is called CIELCh or CIEHLC space. In the cylindrical coordinates,  $C^*$  defines the chroma, and  $h$  the hue angle in degrees (Elliot et al., 2015).

CIELUV color space is an update of the CIEWUV model. This color space implements the same CIELAB  $L^*$ -axis that represents lightness, and the  $u^*$ ,  $v^*$  axes define the chroma, from 0 to 100. The most relevant difference between CIELAB and CIELUV is their chromatic adaptation model. In CIELAB, the values are normalized by dividing by the white point, while in CIELUV, the normalization is done by subtracting the white point (Kahu et al., 2019). Therefore, CIELAB is used with substantive mixtures (e.g., prints) and CIELUV for additive mixtures of colored light (e.g., displays) (Castellano, 2012). As well as in CIELAB, the Euclidean distance between two stimuli coordinates will describe the difference in color appearance (Elliot et al., 2015). The chromaticity diagram derived from the CIELUV color space can be visualized in the Figure 2.3b.

### 2.2.1.2 Common RGB Color specifications

RGB color space is a device-dependent color space. As previously explained (section 2.1), the same RGB input values produce different color appearances depending on the display device. In digital media and visualization, different device-independent RGB-based color spaces have been developed to address this problem. The most common RGB color spaces are sRGB, Adobe RGB, and ProPhoto RGB (Castellano, 2012).

**Table 2.1:** sRGB specifications (Castellano, 2012).

Parameter	Value(s)
Luminance	80 $cdm^{-2}$ for 100% white
White point	D65: (x = 0.3127, y = 0.3291)
Primaries (CIE 1931)	Red: (x = 0.64, y = 0.33), Green: (x = 0.30, y = 0.60), Blue: (x = 0.15, y = 0.06)
Gamma	2.4
Ambient illuminance	64 lx
Ambient white point	D50: (x = 0.3457, y = 0.3585)
Veiling Glare	1%

sRGB color space was proposed as standard by Hewlett-Packard Company and

## Chapter 2 | THEORETICAL BACKGROUND

Microsoft Corporation in the 1996. sRGB tried to approximate the performance of most computer displays to achieve a common RGB response between devices (Rhyne, 2017). Since modern displays often simulate the behaviour of the old computers, sRGB still being the standard color space for encoding images, computer color rendering, or to display images on the Internet (Rhyne, 2017) (Elliot et al., 2015). The sRGB values are defined using a reference display and under a specific viewing conditions(Consortium, 2020). Consequently, is important to consider these specifications to interpret the sRGB values. Table 2.1 shows the mentioned sRGB specifications.

There exists a direct transformation between sRGB and CIE XYZ tristimulus values. This transformation is possible through a straightforward  $3 \times 3$  matrix multiplication. As a result, good color communication between devices is possible by using sRGB (Morovič, 2008).

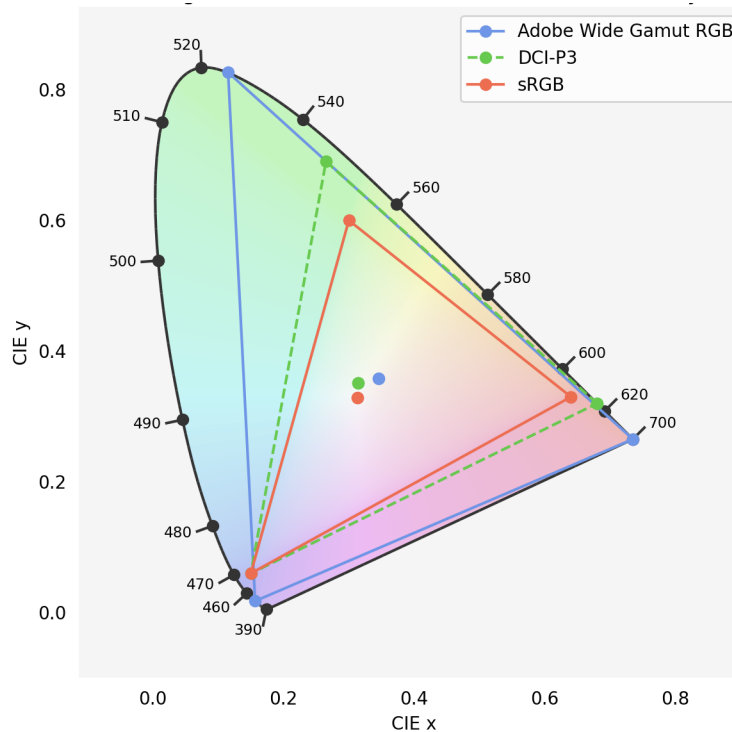


**Figure 2.4:** Adobe Wide Gamut RGB, DCI-P3, and sRGB gamuts representation in the xy chromaticity diagram.

After sRGB, other device-independent RGB-based color spaces were developed for different applications. Adobe RGB was created by Adobe Systems in 1998. This space covers a wider range of colors, allowing a better representation of the colors supported by CMYK printers. Adobe Wide Gamut RGB is the successor of Adobe

RGB, which provides a large gamut, shown in Figure 2.4 (Rhyne, 2017). Another example is Digital Cinema Initiative (DCI-P3), used in digital movie theaters and wide gamut displays (Soneira, 2016). With the development in display technologies, more and more wide gamuts are emerging, adapted to today's ultra-high-definition displays (Elliot et al., 2015).

## 2.2.2 Device-Dependent Color Models

Device-dependent color models are used to represent the digital color values within a specific device. These color values depend on the device and do not contain information about the resulting color appearance (Kang, 2006). Although two devices receive the same device-dependent color values as input, their color output might be mismatched. Thus, these device-dependent color models are useful to control the device color operations and only make sense for a specific uncalibrated<sup>2</sup> device.

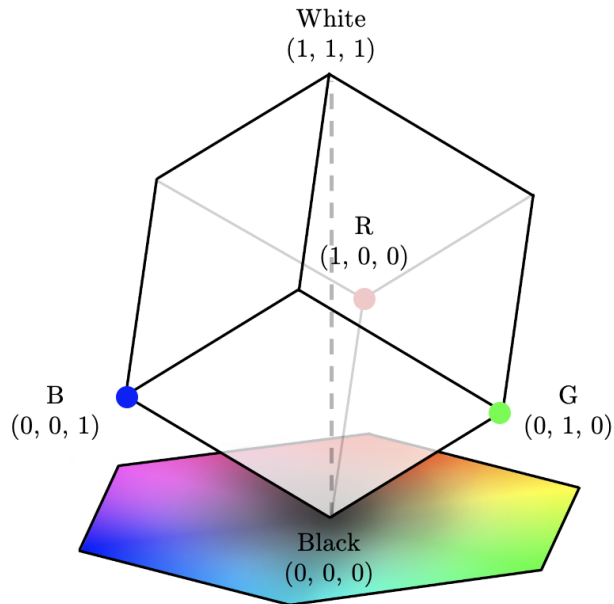


**Figure 2.5:** Representation of RGB color space. The RGB space can be projected to form HSV or HSL. (Illustration inspired by Pigeon (2022).)

RGB color space is the most used color model in digital media. Display

---

<sup>2</sup>Given two perfectly calibrated devices with identical physical properties, the same digital color values will produce a matched color appearance.

technologies are built by pixels based on an RGB set (Red, Green, and Blue). This color space is an additive color-mixing model that contains all the color values within a cube. In the RGB space, a color is represented with three numbers (R, G, B) which determine its location in the three-dimensional space. Each of the three numbers corresponds to one axis of the cube, in a range from 0 to 1 (Rhyne, 2017). The diagonal of the cube, from black (0, 0, 0) to white (1, 1, 1), includes the achromatic colors (Figure 2.5).

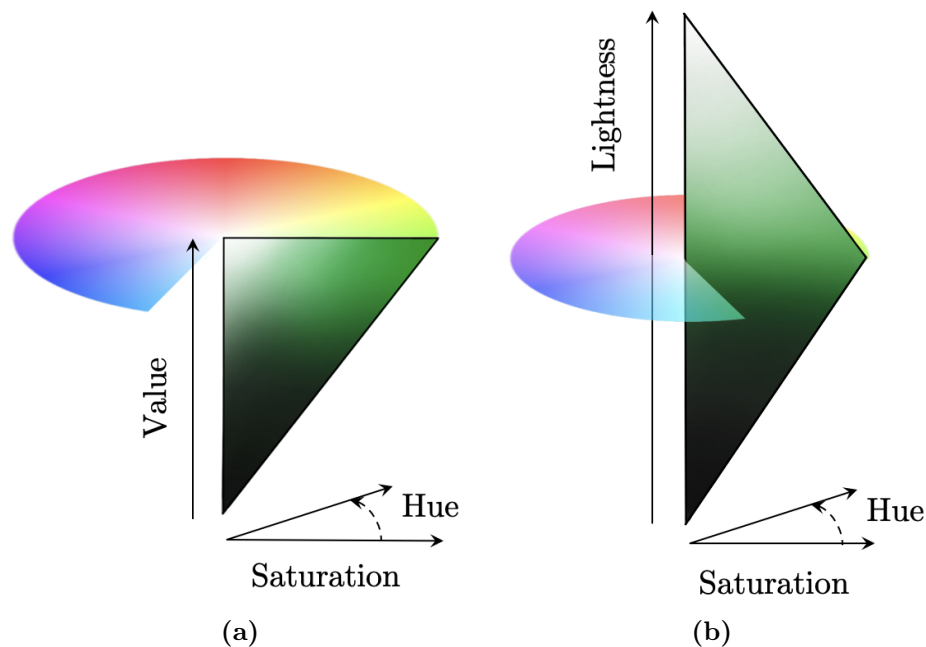


**Figure 2.6:** Schematic representation of HSV and HSL color spaces. (a) HSV color space. (b) HSL color space. (Illustration inspired by Rhyne (2017).)

Hue, Saturation, Value (HSV) and Hue, Saturation, Lightness (HSL) color spaces (Figure 2.6) are simple transformations of the RGB color space (Elliot et al., 2015). These models are intended to be more intuitive and better represent how color additions are perceived. HSV and HSL are frequently used in graphic design software (Rhyne, 2017). Both share the same hue polar coordinates ranging from 0 to 360 degrees. The saturation values have the same interpretation, but their range varies depending on the Value coordinate for HSV and the Lightness coordinate for HSL. In this context, saturation is referred to the radial distance from the neutral grey. The minimum saturation is set as 0, an achromatic stimulus, while the maximum possible is 100. The last coordinates, Value and Lightness, are responsible for the geometry change between the two color models. The Value defines the brightness of the color in the HSV color model, from black (0 units) to

white (100 units). As the Value decreases, the maximum possible saturation range decreases, creating the representative cone shape of the HSV model.

In the HSL color model, the Lightness represents the illumination from no light (0%) to full illumination (100%). The Lightness divides this space into two differentiable parts. All the colors with less than 50% of Lightness are darker than the colors with more than 50%. In HSL, the saturation is maximum for all the colors that are not mixtures between black and white. Then, the geometry of this space can be built as a double cone (Rhyne, 2017).

### 2.2.3 Web colors and Okhsv

In order to obtain a good color reproduction in graphics, the World Wide Web Consortium propose a number of standards to follow on the Web (W3C, 2022). As explained in the subsubsection 2.2.1.2, sRGB is the most common color space used on the Internet. This color space has been standardized since in a common display will result in a close correct color reproduction (Morovič, 2008). However, it is important to emphasize that when the sRGB values are displayed in a device which is not calibrated with the sRGB specifications, its coordinates cannot be described in terms of color appearance and are no longer a device-independent representation.

HSV and HSL color models are the most popular as color selection tools on the web browser given their perceptual connotations, simplicity and low computational cost (Ottosson, 2021b). These spaces are direct transformations from the RGB space, so HSV and HSL are often used together with sRGB. Compared with HSL, HSV color space is more understandable since each parameter corresponds with one color attribute. But unfortunately, HSV is not supported by the standard web content development (e.g., Cascading Style Sheets (CSS)) because of the way it represents mixed colors (Rhyne, 2017).

Since color models like HSV or HSL are not proper color spaces (such as CIELAB or CIELUV), they are far from an ideal homogeneous color space. Consequently, several new color spaces that better represent human color perception have emerged to be used on the web. Two good examples are Okhsv and Okhsl (Ottosson, 2021b), created in 2021. These new models are derived from previous human visual experiment data and they are designed to work with the sRGB gamut. Previously, color spaces such as CIELAB were implemented for their web use. However, these spaces are limited by the sRGB gamut (the standard color space on the web) and their complexity. The irregularity of the sRGB gamut in these complex spaces (see an example in Figure 2.7) easily produces out-of-gamut colors. Moreover, the required specifications, such as viewing conditions, have led to the persistence of

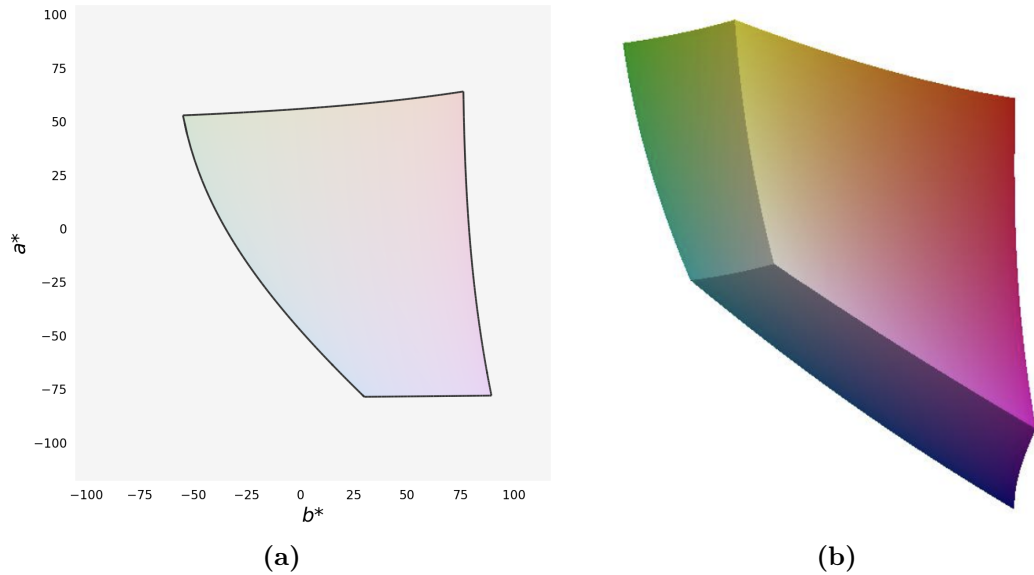


**Figure 2.7:** Visualization of the sRGB irregular shape in the CIELAB color space. (a) sRGB color space section at 50% of lightness in CIELAB. (b) sRGB three-dimensional shape in CIELAB.

HSV and HSL as the most popular color-picker spaces. To solve these drawbacks and replace the old HSV and HSL, Okhsv and Okhsv were created, so they are similar to HSV and HSL but more homogeneous. Thus, Okhsv manages to keep the advantages of HSV but with better color perception representation. The Okhsv improvement, compared with old models, can be visualized in the interactive color picker available in (Ottosson, 2021a).

## 2.3 Display Calibration

Display calibration guarantees accurate color images and allows reliable color communication between devices, for example, achieving the same color appearance on two screens (Consortium, 2022a). To this end, the calibration and characterization output describes the parameters and calculations that map the device-dependent digital signals into device-independent values. This output is saved into the display profile, which can contain  $3 \times 3$  matrix transformation, power-law mapping, white-point normalization, lookup tables (one-dimensional and multidimensional), etc. (Sharma and Bala, 2017)

## 2.3.1 Calibration parameters

To achieve the desired color behavior is important to consider a series of parameters that can be referred to as the calibration parameters. They can be stored in a device profile, which links color between devices. (Sharma and Bala, 2017).

### 2.3.1.1 RGB Primaries

The most common display technology today, liquid crystal display, is composed of three filters, red, green, and blue, which combine to generate colored light (Elliot et al., 2015). Each of the filters individually produces one of the RGB primaries.

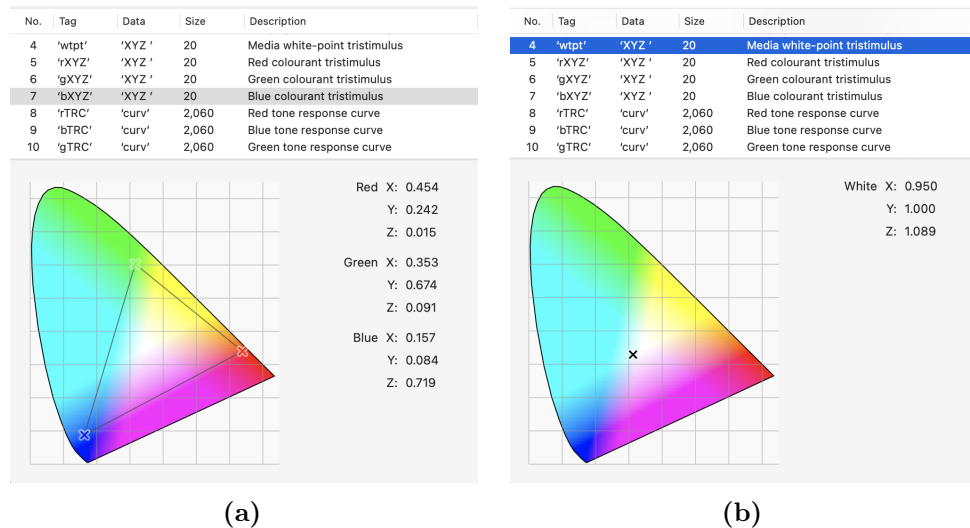


**Figure 2.8:** (a) Coordinates of the RGB primaries in the chromaticity diagram. (b) Profile white point coordinates in the chromaticity diagram. (Screen capture from ColorSync Utility.)

Since different RGB values produce different colors, understanding the primaries will allow for compensating color mismatches (Sharma, 2018). To perform color adjustments, the RGB primaries (device-dependent) must be related to a device-independent color model. Then, the three primaries are saved in the profile in terms of XYZ tristimulus values and are represented as rXYZ, gXYZ, and bXYZ (Figure 2.8a) (Elliot et al., 2015).

The relationship between RGB and XYZ is established during the characterization process and can be presented as a  $3 \times 3$  matrix calculation. This matrix, together with gamma correction, converts the RGB values into XYZ (developed in subsection 2.3.3) (Sharma, 2018).

### 2.3.1.2 White point

White point is of particular importance since the visual system interprets colors based on a neutral reference, which is considered white. Changes in the white point on an image will suppose changes in the appearance of the surrounding colors. During the calibration process, it is possible to set the display's white point using as reference a standard illuminant, such as D50 or D65. The changed white point is saved in the profile using XYZ coordinates (wtpt) as Figure 2.8b shows (Fraser et al., 2002).

### 2.3.1.3 Gamma value

The relationship between the input voltage and the resulting light intensity is nonlinear in displays. Typically, this relationship can be approximated using a simple transfer function for old CRT displays (Equation 2.2). In LCD displays, the electro-optic response often follows an S-shaped curve. However, this curve is usually modified to mimic CRT behavior and simplify LCDs signal-to-light-intensity function (Sharma and Bala, 2017).

$$\text{Light-intensity output} = (\text{gain} \cdot \text{input voltage} + \text{offset})^\gamma, \quad (2.1)$$

$$\text{Light-intensity output} = \text{input voltage}^\gamma. \quad (2.2)$$

where  $\gamma$  is the exponent of the power function, called monitor gamma. Displays set the gamma value between 2.0 and 3.0 (Sharma, 2018). For appropriate setup of the display, the offset term becomes 0, and since  $\text{gain} = (1 - \text{offset})$ , the Equation 2.2 can be simplified into the Equation 2.1 (Sharma and Bala, 2017).

The gamma value modulates the channel intensity function used to characterize displays, called Tone Reproduction Curve (TRC). The TRC can be different for each channel (rTRC, gTRC and bTRC). Together with the XYZ values of the RGB primaries, TRCs data is employed to compute the transformation between device-dependent and device-independent color representations (Sharma and Bala, 2017).

Gamma value can produce changes in the contrast perception. A high gamma value will give a flat appearance or lack of contrast, while a low gamma value will generate a high-contrast image with detail loss as Figure 2.9 shows (W3C, 1996).

### 2.3.1.4 Luminance

Luminance value quantifies the amount of light which is emitted by a display and is measured in  $\text{cd}/\text{m}^2$ . One of the requirements for a color displayed on two different

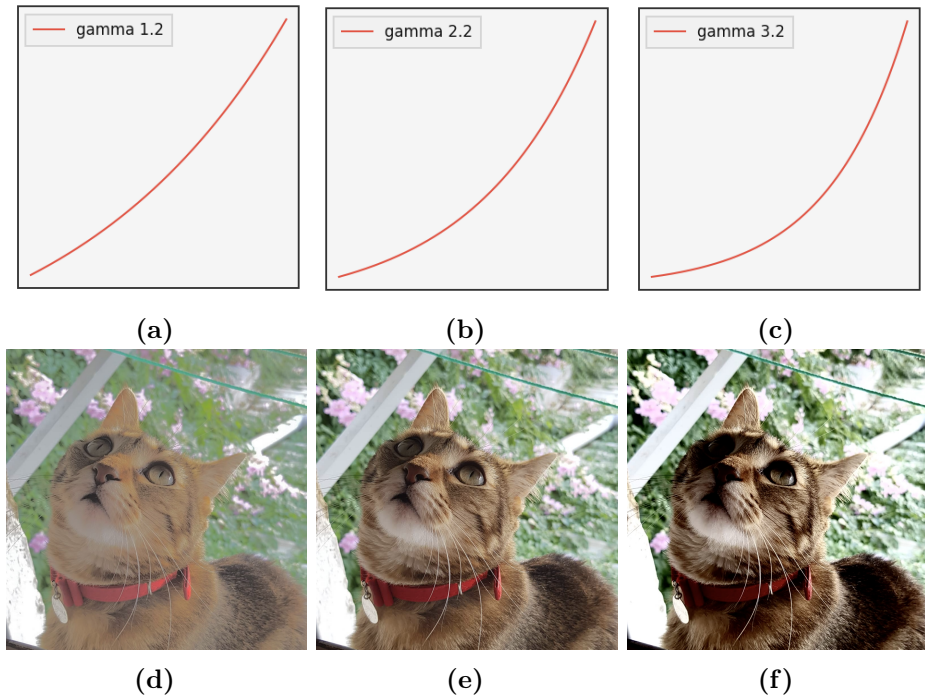


**Figure 2.9:** Gamma value changes the contrast appearance. Low gamma, (a), generates a low-contrast image, (d). Normal image, (e), and standard gamma, (b). High gamma, (c), produces a high-contrast image, (f).

screens to match is that it has the same luminance in both devices. Thus, the luminance value must be controlled and specified to ensure that a color has the desired appearance (Sharma, 2018).

### 2.3.2 Calibration accuracy limitations

The calibration results are influenced by three main factors: viewing conditions, measurement instrument, and observer metamerism. The viewing conditions affect how a stimulus is perceived. For example, changes in the lighting environment will suppose a change in the color appearance of an image. Then, a calibrated display is subject to the conditions under which it was performed. Another factor to consider is the measurement instrument, which is referred to the device that collects color measurements of the display. An ideal measurement instrument will give accurate and reproducible results. In this sense, telespectroradiometers are the best choice. The last factor, observer metamerism, involves the differences in terms of visual perception between users. Variations in the color perception can

produce color mismatched between displays (Consortium, 2022a).

### 2.3.3 Display Characterization

The correlation between the digital input values and their corresponding appearance output is established during the characterization process for a calibrated display. Therefore the characterization gives the mathematical relationship between the device-dependent values and their correspondent device-independent representation (for example, XYZ tristimulus values) (Sharma and Bala, 2017).

The characterization is commonly completed by taking measurements that verify a correct transformation between the device-dependent and device-independent values. The values are collected using measuring instruments such as colorimeter or spectrophotometer (Sharma, 2018). However, there also exist visual approaches that derive this transformation (section 2.4).

There are three different characterization approaches: physical, empirical, and hybrid models. Physical models define the physical process that uses the display to reproduce color. In this approach, the parameters are calculated using a small number of measurements, being simpler than in other models (Consortium et al., 2004). Physical-based methods are divided into two stages. First, the device-dependent values are changed into device-dependent linearized data by using TRCs. Second, device-dependent linearized data are transformed into device-independent, where it is required at least a  $3 \times 3$  transformation matrix (Equation 2.3) (Sharma and Bala, 2017). An example of a frequently used physical characterization is the GOG model (Barnard and Funt, 2002).

$$\begin{bmatrix} X \\ Y \\ Z \end{bmatrix} = M \begin{bmatrix} R' \\ G' \\ B' \end{bmatrix}, \quad (2.3)$$

$$\begin{bmatrix} R' \\ G' \\ B' \end{bmatrix} = M^{-1} \begin{bmatrix} X \\ Y \\ Z \end{bmatrix} \quad (2.4)$$

where  $M$  is the matrix that transforms the  $XYZ$  tristimulus values into the linear-RGB ( $R'G'B'$ ), and  $M^{-1}$  is the inverse transformation of  $M$ , that convert  $R'G'B'$  into  $XYZ$  values.

On the other hand, empirical-based models need a large number of measurements, and they are utilized to perform data-fitting or interpolation operations. The measurements are directly correlated with their correspondent device-dependent values (Sharma and Bala, 2017). This method can be performed together with

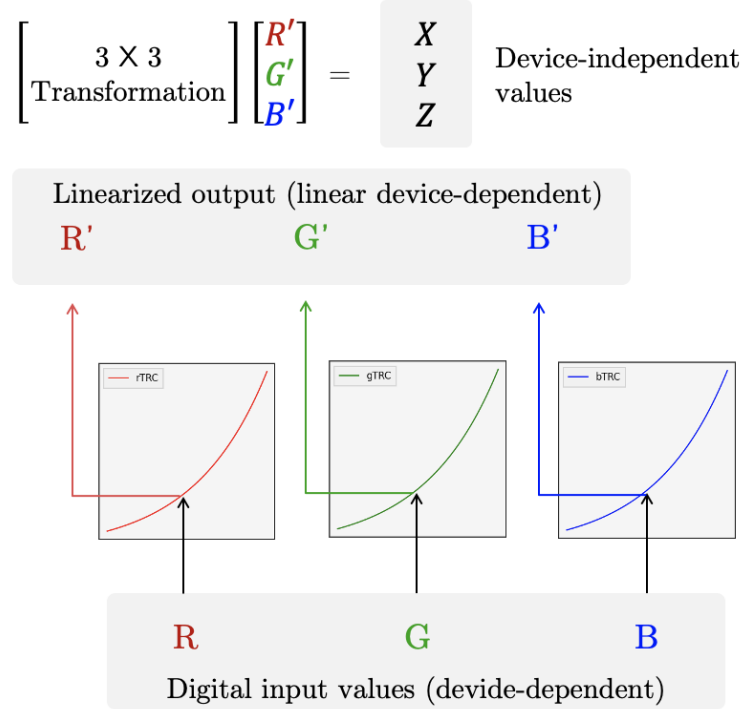


**Figure 2.10:** Characterization process based on physical model. The RGB input is linearized before compute the transformation that convert R'G'B' into CIE XYZ tristimulus values. (Illustration inspired by Giorgianni and Madden (2008))

simple calibration or characterization (Consortium et al., 2004). Look-up tables, least-squares linear and polynomial regression, and neural networks are some examples of this method. Look-up tables store the display input values and their correspondent output values to describe the relationship between the two color spaces. In polynomial and linear regression models, it is assumed the relationship between the input and output values, performing a polynomial and linear mapping respectively between both values. Recently, machine learning approaches such as support vector machines or artificial neural networks have emerged as new alternatives (Amani et al., 2019). Practically, hybrid models, which are the methods that combine the strengths of physical and empirical models, are the most used approaches in characterization since they give the best performance (Consortium et al., 2004).

## 2.4 Review on visual display calibration

Calibrating displays with visual approaches usually consists of varying a stimulus until it matches a reference with known values. When the selected stimulus and the reference match, it is obtained the value that relates the digital values of the device to its visual appearance. Thus, the human visual system acts as a measurement device. Although the human visual system can play the role of a measuring instrument, there are some drawbacks, such as the task difficulty (it does not allow a large number of measurements) or the inter-observer variations. Nonetheless, visual approaches are selected when performing an instrumentation-based calibration is not possible. Measurement instruments are not always available and usually require previous knowledge about calibration.

There are different visual techniques used to estimate the parameters of a display. To estimate gamma value has been proposed several methods with different approaches. Kay and Brandenberg (2007) obtain the gamma parameter by matching two patches in terms of luminance. Braun (2003) uses flicker photometry techniques. Mulligan (2009) obtained gamma by a motion-nulling method utilizing half-tones as stimuli. Additionally, Xiao et al. (2011a) proposed a method to obtain the gamma value on LCD displays by visually matching a half-tone background with a uniform patch. For the luminance parameter, techniques similar to those of gamma value have been employed. Braun (2003) also applies the flicker photometry to estimate the channel luminance ratios. Anstis and Cavanagh (1983) first proposed the motion-nulling technique that Mulligan (2009) used as reference to implement their gamma estimation method. In this case, the relative luminance is estimated, and the stimuli are red-green stripes spatially alternated with yellow-brown stripes. Moving on to color parameter, there are two main approaches, based on unique hue judgments and based on a physical reference match. Karatzas and Wuerger (2007) proposed a color calibration method that uses unique hue judgments data to define the display color properties. These judgments are supposed to be approximately constant across the population and the task easy to perform (e.g., choose a colored light such that it appears neither red nor green). From the experiments is derived the transformation matrix, which adjusts the pixel values of the display to achieve the desired color appearance. In a different approach, Mulligan (2009) performed color matches using as reference a dollar bill. The chromatic values of the bill were previously measured. In this method, the color transformation is computed using the known values from the dollar and the pixel values after the match.

Recently, open source softwaers are also available that perform the calibration process combining some of the previously mentioned techniques to calibrate several display parameters (Ban and Yamamoto, 2013).

# 3 | Data collection

This chapter describes the conducted psychophysical experiments and the collected specific-display data. A GUI for selecting pure hues and a neutral background was developed.

## 3.1 Experimental Interface design (Stimuli)

We designed an experimental interface that was utilized in two tasks. First, it was shown to select the neutral grey of the display devices used in our experiment. Next, the interface was employed to conduct hue judgments. In this section, we explain the common features between both stages, although they are slightly different from each other, explained in more detail in the section 3.3 and section 3.4.

To implement the Graphical User Interface (GUI), we used JavaScript, CSS, HTML, and the framework jsPsych (jsPsych, 2022) (a framework for creating experiments that run in a web browser). These tools were selected since we intend to make a GUI that is available for every device and can be run online.

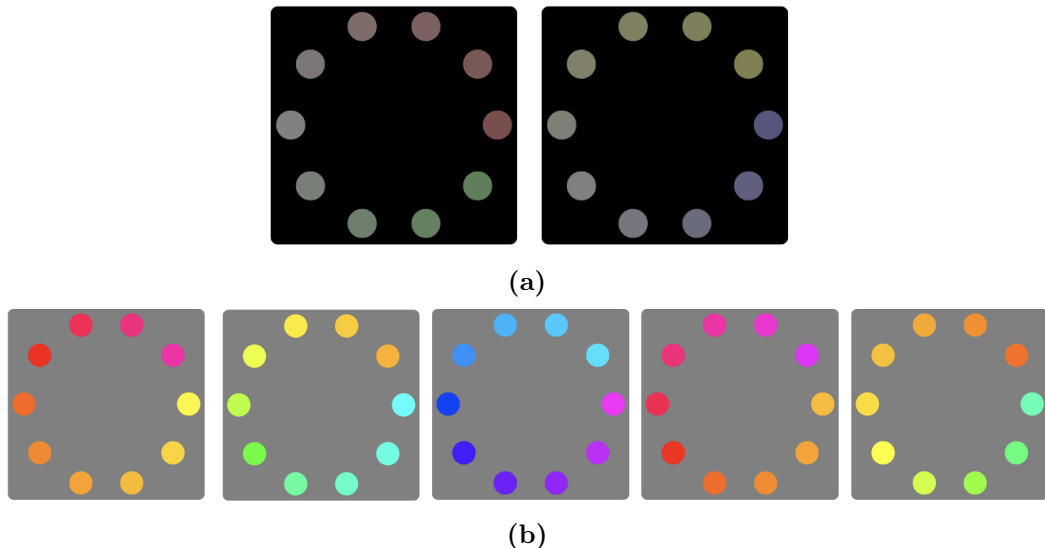


**Figure 3.1:** (a) Neutral grey stage, divided into 2 tasks (neutral grey along the red-green axis and along the yellow-blue axis). (b) The hue judgments stage is divided into 5 tasks (red, green, blue, orange, and yellow hue selections).

The stimulus shown formed an annulus of 10 selectable patches. At 60 cm, the diameter of the annulus was 12°, and the patches were presented with a visual

angle of  $2^\circ$ . The observer selected the target stimulus by a mouse press on the patch. Once the patch was selected, the next trial automatically started.

Two rotations were introduced between each trial (Figure 3.2). First, a  $12^\circ$  rotation is applied so that the stimuli are placed in the space between the previous patches. The purpose of this rotation is to mitigate the effect of successive contrast<sup>1</sup>. The following rotation starts from the previous position, but this time the annulus is rotated a random number of times at  $36^\circ$ . This rotation ensures a random starting position for the annulus, covering different screen parts.

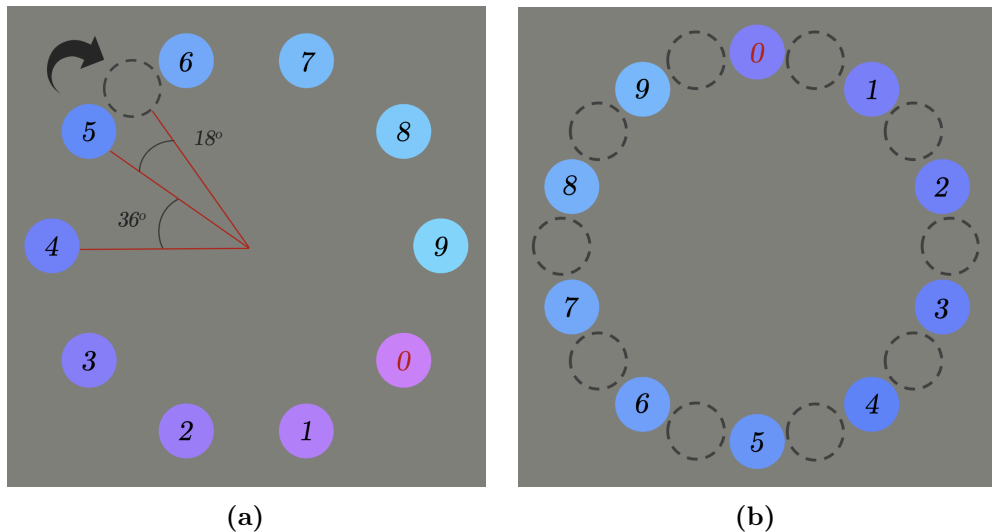


**Figure 3.2:** Two rotations are introduced between consecutive trials, such as (a) and (b). First, the stimuli are rotated  $12^\circ$  to place them in the space between previous patches (the dashed lines indicate this rotation). Once the stimuli are in this position, the annulus is randomly rotated  $36^\circ$  times (the numbers indicate the second rotation).

In both tasks, neutral grey and hue selections, the color patches are displayed in an ordered fashion (Figure 3.1). In (Xiao et al., 2011b), Xiao *et al.* experimented with a similar interface where they implemented the annulus colors following two arrangements, a random disposition, and an orderly disposition. After the experiments, they observed that the mean hue angles were the same for both arrangements, but in the random arrangement, the observers took more time to respond and perceived it as more complex. As our visual calibration process aims to be accessible and easy for every user, we decided to implement an orderly arrangement in our experiments.

<sup>1</sup>Successive contrast is the phenomenon by which the appearance of a stimulus is modified by a previous stimulus located in the same area when the two stimuli are visualized consecutively (Castellano, 2012).

## 3.2 Experimental Methodology

Thirteen participants took part in the experiment (9 males and 3 females; mean age: 26 years; age range: 21-51 years). All observers had normal color vision assessed using the Ishihara test under D50 illuminant. The subjects were seated in a dark room in front of a computer display at a distance of 60 cm.

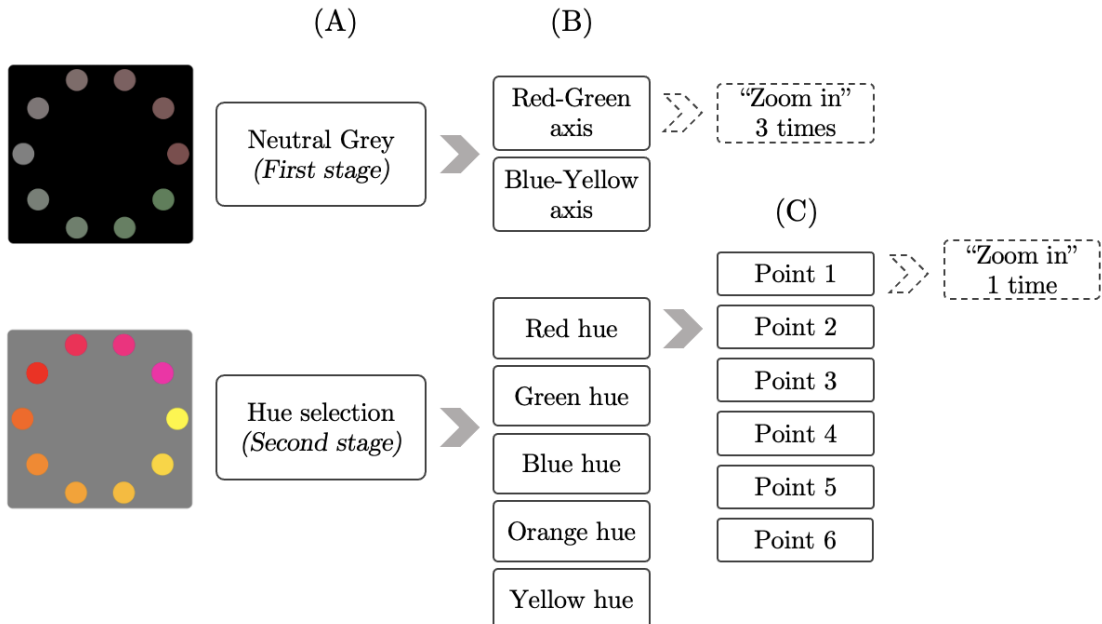


**Figure 3.3:** (a) The complete experiment is divided into 2 stages. (b) The neutral grey stage is divided into 2 tasks; each task has 4 trials ( $1 + 3$  "zoom in"). The hue selection stage is divided into 5 tasks according to the five different hues. (c) Within a hue selection task, there are 6 Saturation/Value combinations (six points). Each point has 2 trials ( $1 + 1$  "zoom in").

Before beginning the experiment, the instructions for the entire process were given to the participants. They also were informed that the task was subjective and that there was no right or wrong answer. Moreover, for each selection, written instructions were shown in the upper left corner of the screen. During the experiment, the participants were asked to do different judgements according to the stage. In the neutral grey stage, the settings were to select a neutral grey, whereas in the second stage, the subject was asked to select a pure hue, for example, "a red that is neither blue (like red-magenta) nor yellowish (like yellow-red)" (the instruction are more detailed in the section 3.3 and section 3.4).

The neutral grey and hue selection stages combined add up to 68 judgments. For each of the 5 hues displayed during the second stage, the subjects selected

12 patches, a total of 60 assessments ( $5$  hues  $\times$   $6$  saturation/value combinations (section 3.4)  $\times$   $2$  trials). The first stage adds  $8$  more assessments ( $2$  hue axes combinations  $\times$   $4$  trials). Both stages in a session lasted  $\sim 15$  min. In Figure 3.3 can be visualized the workflow of the complete experiment.

### 3.3 Neutral background stage

Since the assumption that the same proportion of the R, G, and B channels produces neutral grey is not necessarily correct for an uncalibrated device (Karatzas and Wuerger, 2007), and the color appearance depends on the surrounding colors, it is essential to define an achromatic background (Gerrits and Vendrik, 1970). Following the opponent-color theory, the red-green and the yellow-blue channels are at equilibrium when a color-normal observer views an achromatic stimulus (Hurvich and Jameson, 1957).

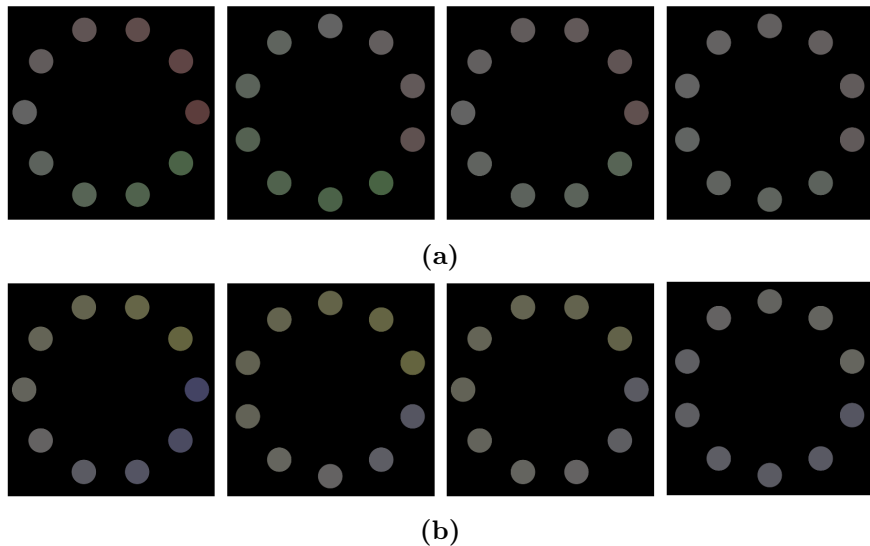


**Figure 3.4:** There are  $4$  trials within each task, allowing a precise neutral grey selection. Consecutive trials make the saturation values between patches closer. (a) First task, along the Red-Green axis. (b) The second task, along the yellow-blue axis.

In their study, Chauhan et al. (2014) verify that the intra-observer and inter-observer variability is reduced by adjusting the light along the red-green and the yellow-blue axes compared to adjustment along the main axes of the CIE  $u^*v^*$  chromaticity diagram. Then, according to the results from Chauhan et al. (2014) and Karatzas and Wuerger (2007), we determine the achromatic background by

shifting the hue along the red-green and the yellow-blue axes in the HSV color space. During our experiment, the user was able to choose an achromatic stimulus with an increment of saturation along the hue angles of  $0^\circ$ - $120^\circ$  (red-green axis) and  $60^\circ$ - $240^\circ$  (yellow-blue axis) Figure 3.4.

The two pairs of hue angles (red-green and yellow-blue) divide the neutral background stage into two main tasks. Each consists of 4 trials where the steps of saturation decrease around the previous stimulus selection (Figure 3.5). These stimuli were displayed on a black background (pixel values set to 0).

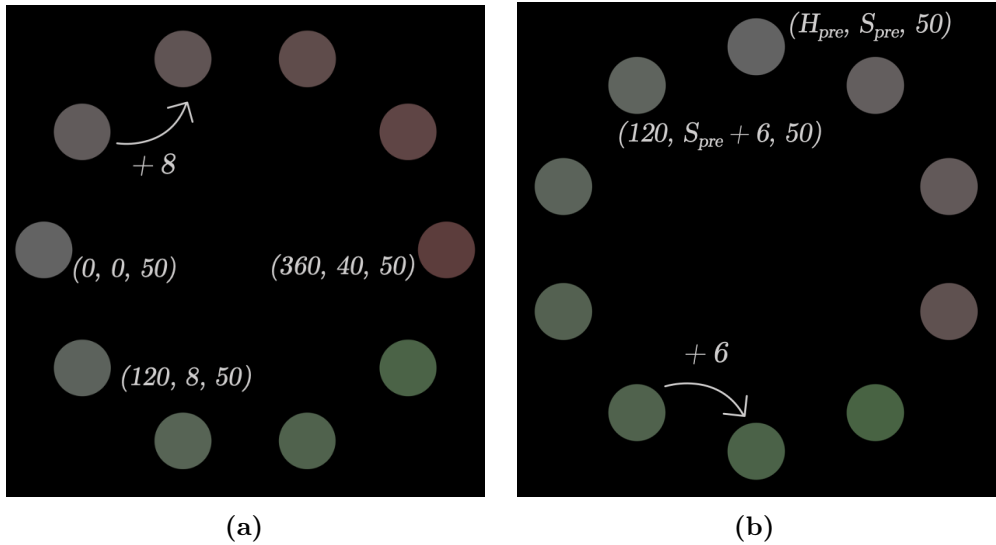


**Figure 3.5:** Saturation arrangement between consecutive trials. (a) First trial. From the theoretical neutral grey HSV(0,0,50), the saturation increase between patches in 8 units. (b) Second trial. The saturation values get closer around the previously selected patch (steps of 6 saturation units).

In the first displayed trial, within the first task (neutral grey along the red-green axis), the annulus (section 3.1) was arranged according to two hue angles, five or four levels of saturation (depending on the hue start position), and a fixed value (value 50 in HSV). Halfway around the annulus, we place the theoretical neutral grey (HSV: [0,0,50] coordinates). From the theoretical neutral grey position, the saturation increases in 8-unit steps, on a scale of 0-100. This increment follows a clockwise direction for the red hue and a counterclockwise direction for the green hue (Figure 3.5a).

In the second trial, the previously selected patch,  $(H_{pre}, S_{pre}, 50)$ , appears in the new annulus in a random position to prevent the color arrangement from introducing any bias in the selection. The saturation steps increase around  $(H_{pre}, S_{pre}, 50)$ , but this time, in steps of 6 units (2 units less than the first trial). Consequently, a

“zoom in” effect was achieved so that the participants could select a more precise neutral grey. This “zoom in” was repeated 3 times, while the hue angles and value (HSV) were preserved throughout the task.

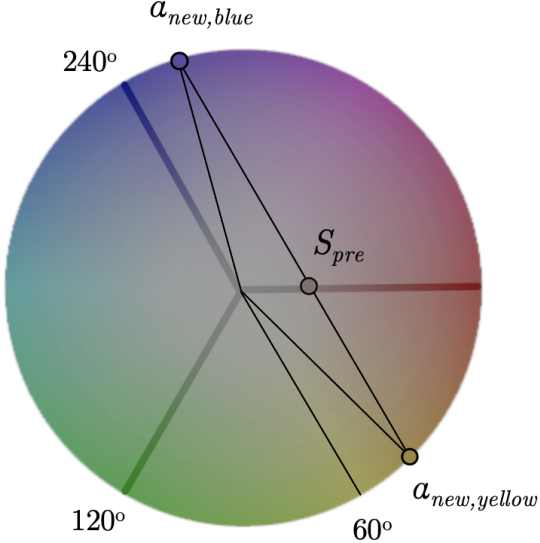


**Figure 3.6:** Visualization of the new hue angles calculation in the HSV color model. The center of the wheel represents the theoretical neutral grey, HSV: (0,0,50).  $S_{pre}$  is the previously selected saturation which in this case is towards the red hue. The two new hue angles,  $\alpha_{new,yellow}$  and  $\alpha_{new,blue}$ , are derived from  $S_{pre}$ .

Moving on to the second task (neutral grey along the yellow-blue axis) is important to note that the two displayed hues depend on the selection made in the previous task. These hues are calculated considering the yellow-blue axis in the HSV color space by using the Equation 3.2 and Equation 3.3). Figure 3.6 illustrates how the new angles are obtained.

$$\frac{S_{max}}{\sin 120^\circ} = \frac{S_{pre}}{\sin(60^\circ - \alpha_{new,yellow})}, \quad (3.1)$$

$$\alpha_{new,yellow} = 60^\circ - \arcsin\left(\frac{S_{pre} \sin 120^\circ}{S_{max}}\right), \quad (3.2)$$

$$\alpha_{new,blue} = 120^\circ - \alpha_{new,yellow} \quad (3.3)$$

where  $\alpha_{new,yellow}$  and  $\alpha_{new,blue}$  are the new hue angles in the HSV color space.  $S_{pre}$  is the previously selected saturation, towards red or green hues, and  $S_{max}$  is the maximum possible saturation which is 100 units in the HSV color model.  $120^\circ$  and

$60^\circ$  are the green and yellow hue angles respectively. The rest of the second task follows the same steps as the first one.

The hue, saturation, and value settings can be summarized as follows:

- Hue arrangement: the hue changes per task. In the first task, one half of the annulus is red (HSV  $0^\circ$ ) and the other is green (HSV  $120^\circ$ ). In the second task the hues depend on the previous selection and they are calculated along the blue (HSV  $240^\circ$ ) and yellow (HSV  $60^\circ$ ) axis.
- Saturation arrangement: within each trial, the saturation increases between patches halfway across the annulus in a clockwise and counterclockwise direction. Moreover, the saturation is also decreased between trials.
- Value arrangement: the value is constant throughout the process (value 50 in HSV).

The output from the experiment is adopted as the new neutral grey of the specific device, and it was employed as background in the following stage (hue selection: section 3.4). This grey is also used in one of the transformation matrices to preserve the white point (subsection 4.5.3).

## 3.4 Hue selections stage

In the second stage of the experiment, the interface adopted was similar to the previous trial (section 3.3). However, in this case, the main purpose is to make hue selections. This step contains 5 tasks: judgments over the four unique hues (red, green, blue, and yellow) and orange (subsection 3.4.1). Based on the references (Xiao et al., 2011b), (Bosten and Boehm, 2014) and (Matthen, 2020) we set the instructions as follows:

- Red: neither Bluish (like Red-Magenta) nor Yellowish (like Yellow-Red).
- Green: neither Yellowish (like Green-Yellow) nor Bluish (like Cyan-Green).
- Blue: neither Greenish (like Cyan-Green) nor Reddish (like Magenta-Blue).
- Orange: neither Reddish (like Red) nor Yellowish (like Yellow).
- Yellow: neither Greenish (like Green-Yellow) nor Reddish (like Yellow-Red).

The hue selection stage collects the hue judgments to be used to define the hue planes in a psychologically-defined three-dimensional color space. Using HSV color space as reference, the hue planes are contained in a cone where the Saturation

and Value axes define the plane for a specific hue (Figure 3.7). Then, to correctly determine the plane for a particular hue, it is necessary to find at least three hue points in the Saturation/Value-plane. Therefore, on a particular hue selection trial, within a hue task, the Saturation and Value levels are constant and only changes the hue. After repeating the hue trial for different combinations of Saturation and Value levels, the selected hues will define the hue plane.

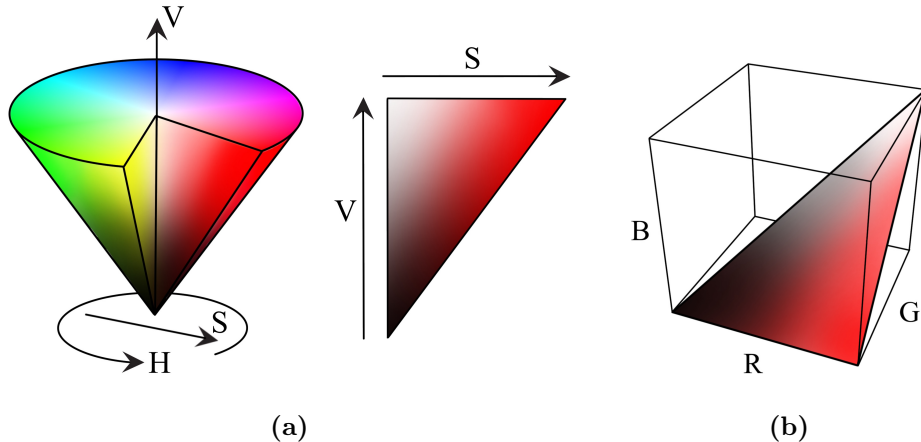


**Figure 3.7:** (a) Visualization of the red hue plane in the HSV color model. H, S and V are the Hue, Saturation and the Value dimensions respectively. (b) Hue plane in the RGB color space.

To precisely estimate the locus of each hue and keep the lowest number of selections, the color space is sampled using six Saturation-Value combinations (Karatzas and Wuerger, 2007). To do a good sampling of the plane and avoid extremely dark patches that make the selection task more complex, we choose the coordinates shown in Figure 3.8 and Table 3.1. Since 5 hues are shown, and 6 points per hue, the result is 30 trials.

**Table 3.1:** Selected Saturation-Value combination points to sample a hue plane. The hue has to be constant to define the plane, and it will take values around 0, 120, 240, 60, or 30 degrees of hue in the HSV color space.

Hue (degrees)	Saturation	Value
0 / 120 / 240 / 60 / 30	100	100
0 / 120 / 240 / 60 / 30	67	100
0 / 120 / 240 / 60 / 30	33	100
0 / 120 / 240 / 60 / 30	100	50
0 / 120 / 240 / 60 / 30	67	50
0 / 120 / 240 / 60 / 30	33	50

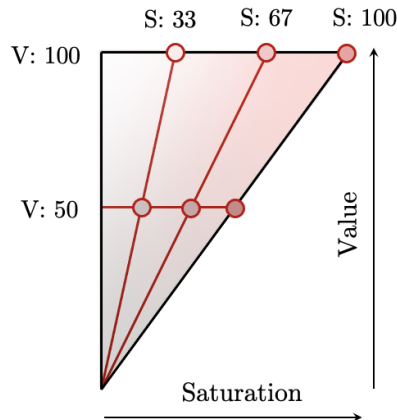


**Figure 3.8:** Value and Saturation (HSV color space) selected coordinates to define a hue plane.

On each Saturation-Value trial, following the selection of the subject, the annulus of hues "zoom in" around the previously selected hue, spanning only  $32^\circ$  of the hue circle in Okhsv color space (subsection 3.4.2). This "zoom in" is done once per hue plane point (2 trials per point). In addition, the selected hue appears in this new annulus in a random position to prevent subjects from choosing the hue halfway through the annulus.

At the end of the experiment, the Okhsv and RGB coordinates of the selected hues are stored in the data file that serves to construct the profile which characterizes the display color properties. Moreover, the selected color patches were re-displayed and measured with the CS-2000 Spectroradiometer from Konica Minolta (Minolta, 2022).

### 3.4.1 Binary hues

Binary hues are referred to as the hues resulting from mixtures of unique hues, for example, orange, which is formed by a mixture of red and yellow (unique hues) (Arstila, 2018). The existence of behavioral evidence that distinguishes unique hues from binary hues is still an open question. According to previous studies (Bosten and Boehm, 2014) (Bosten and Lawrence-Owen, 2014) (Wool et al., 2015) (Arstila, 2018) (Witzel and Gegenfurtner, 2018) the phenomenological, psychophysical, and neurophysiological facts does not support the existence of unique hues or binary hues, and therefore the differences between them in terms of phenomenological experience. Considering these results, we decided to implement a binary hue to analyze how it performs compared with unique hues.

Since our final goal is to obtain an accurate calibration method applicable to all displays and users, and if we consider there is no particular advantage in the use of unique hues, the most logical option would be to search for the hues that induce the least inter- and intra-observer variability. Then, since orange is one of the hues with the reported lowest variance within and between observers (Boston and Lawrence-Owen, 2014) (Forder et al., 2017), we included orange together with the four unique hues (red, green, blue, and yellow) in the hue selection stage.

### 3.4.2 Color spaces

In an online calibration method is important to consider the web browser color space and the available RGB-based color spaces in the web development tools, such as CSS. HSV is a more intuitive color space (one parameter per color attribute) compared with other RGB-based spaces such as HSL. However, HSV is not supported by the standard web content development (subsection 3.4.2). Then, in our GUI, we implement the transformations between HSL and HSV color space to show the stimuli during the neutral grey stage.

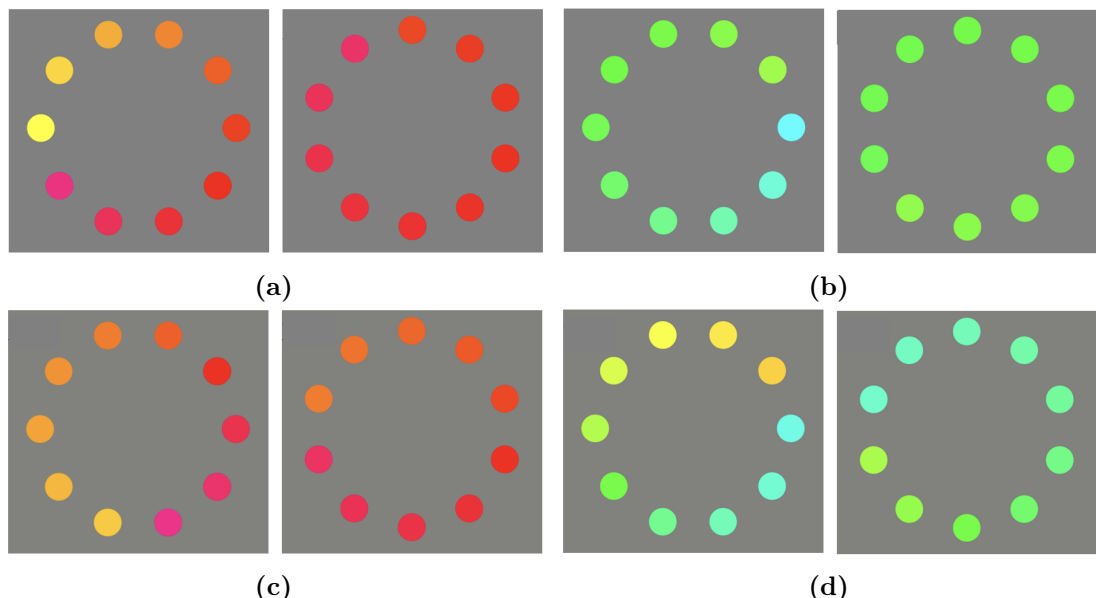


**Figure 3.9:** Visualization of the hue changes between consecutive patches for the red and green hues in the HSV, (a) and (b), and Okhsv, (c) and (d), color spaces. The exact same hue changes are implemented in both color spaces.

In contrast to the grey stage, where only a pair of hues per task was used, a set of 10 different hues were displayed per trial in the hue selections stage. Thus,

to cover the same range of hue angles for each task (red, green, blue, yellow, or orange hue), a consistent hue shift between consecutive patches is necessary. Even though the HSV color model intends to be an intuitive system based on perceptual dimensions (Smith, 1978), it does not conform to human perception in a significant way. Therefore, to use a model that better matches human color perception so equally space hue changes, we implemented the Okhsv color space. This color space is described in more detail in subsection 3.4.2. Compared with the HSV model, Okhsv is derived from previous color perception experiments being a more homogeneous color space.

The Figure 3.9 shows how the implementation of the Okhsv color space improves the homogeneity of the hue angle spacing between patches compared with HSV. For the same hue changes, it is noticeable that the red annulus in HSV covers a wider hue range of hue compared with the green annulus in the same color space. The differences between the green patches are almost unnoticeable in the figure on the right of Figure 3.9b. Moreover, hue changes are abruber in some transitions, for example, in the figure on the left of Figure 3.9a. Instead, using Okhsv, the hues are progressively changing to the same degree, so the covered hue ranges are similar for all the hues, such as illustrated in Figure 3.9c and Figure 3.9d.

# 4 | Calibration Method

This chapter describes the calibration process performed to achieve the same color appearance between two displays. Also presented are the three types of computed matrix-based transformations, which use device profiles created from the previously collected experiments. Additionally, the LCD profiles used to simulate three different displays are explained.

## 4.1 Display Calibration Process

The calibration method aims that two displays seem to match in terms of color appearance without using a measurement device. To this end, a display is color calibrated with respect to another display (reference display) by performing visual judgments that replace the measurement instrument. A set of color patches of similar hue are presented on the display where the task of the observer is to select the patches that appear as pure hues<sup>1</sup> along different hue ranges. In our experiments, the hue ranges were distributed along red, green, blue, yellow and orange. In chapter 3 are explained in detail the conducted psychophysical experiments.

The device profiles that characterize the color behavior of the display are derived from visual judgment data. These judgments must be performed for the user and reference display, which results in two profiles which save a set of display calibration parameters. Using both device profiles is possible to compute the transformation that adjusts the pixel values in the user display to make its color appearance match the reference display.

In the last stage, the transformation is applied to the user display, so the linear RGB values are converted to achieve the desired color behavior. Note that this transformation is computed and applied in the linear device-dependent space. Then, it is required to perform a previous transformation to obtain the linear device-dependent RGB values from the device-dependent RGB.

To summarize, the calibration process can be divided into four main steps (Figure 4.1). First, hue judgments are collected for a specific display device. Second, the reference and user display profiles that describe their color properties are created from the data. Next, the profiles are used to compute the transformation that converts the user display colors to match the reference display colors. Last, the

---

<sup>1</sup>In this project, we call pure hues to the unique hues (red, green, blue and yellow) and binary hues (mixtures of pure hues such as orange or purple). For example, a pure orange will be an orange hue neither reddish nor yellowish, and a pure red will be red neither bluish (like red-magenta) nor yellowish (like yellow-Red).

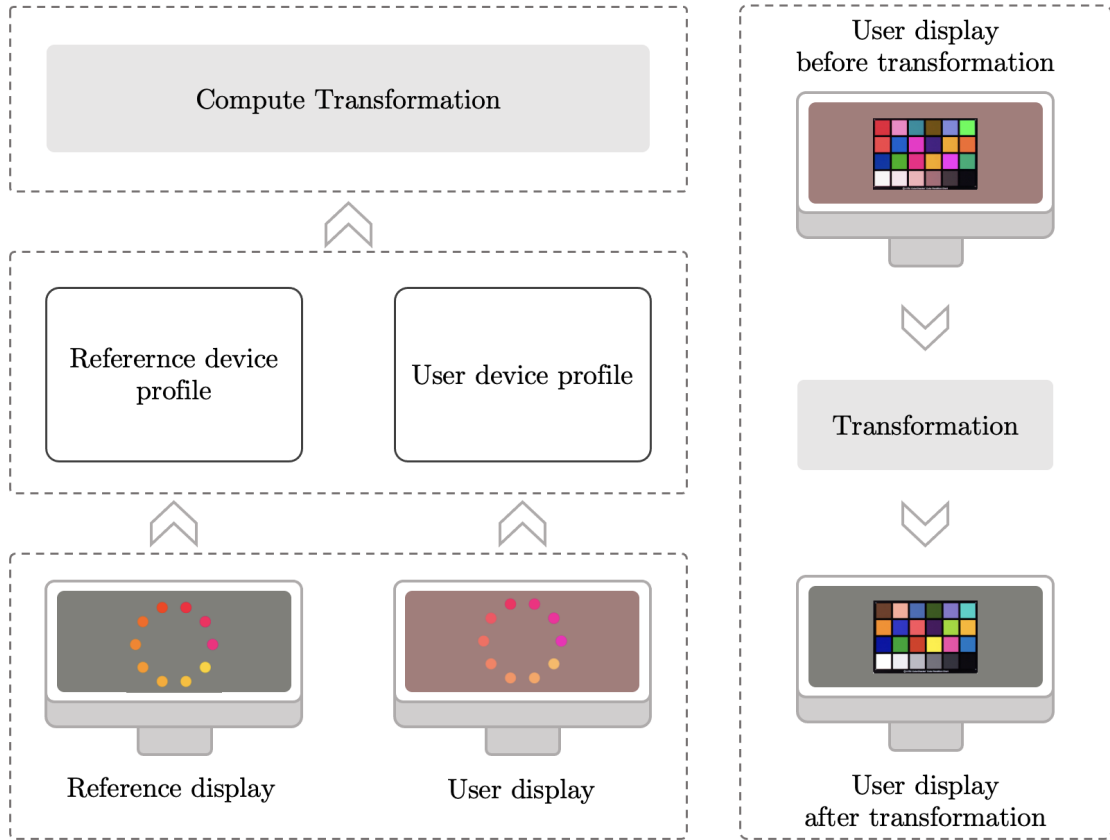


**Figure 4.1:** Calibration workflow. This process can be divided into four main stages.

transformation is applied to the user display; thus, the target colors are obtained.

## 4.2 Display Calibration Methodology

As explained in the previous section, the calibration process starts with the generation of visual judgment data, which is collected through psychophysical experiments. Our experiments were conducted on an Eizo ColorEdge CG279X LCD display (Eizo, 2022) to which three different previously designed profiles were applied. Each profile simulates an independent display with the same physical characteristics but different calibrations (subsection 4.2.2). Thus, three sets of hue data are obtained, one per profile.

The calibration method was applied using seven different settings: three matrix-based transformations (section 4.5), two hue combinations, and two conversions.

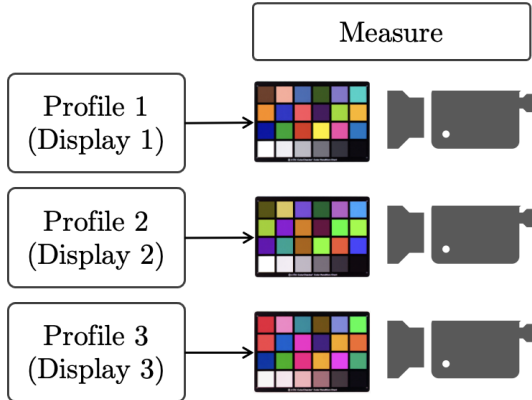


**Figure 4.2:** Measurements were taken for the ColorChecker displayed in the three designed profiles. Each profile simulates a different display.

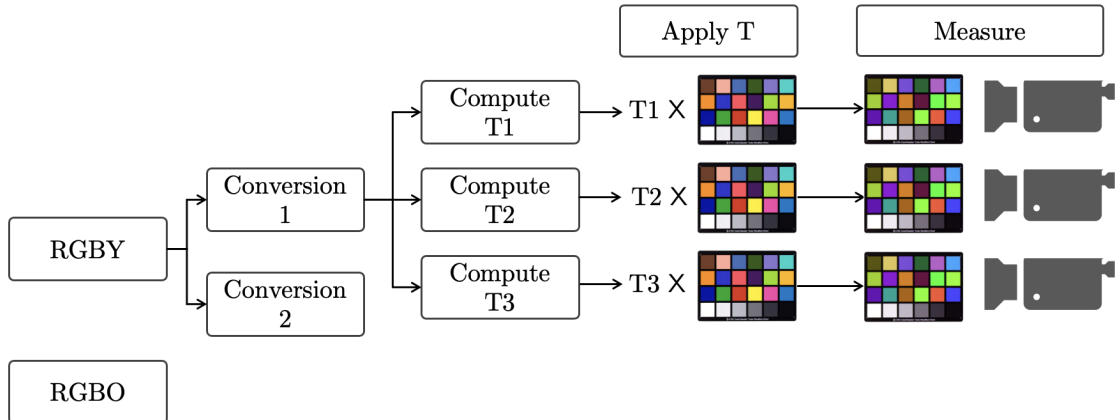


**Figure 4.3:** Visualization of the measurement workflow.

From the psychophysical experiments, the data of six observers were randomly selected. The calibration was applied to the 24 patches of the ColorChecker (Pascale, 2006). Therefore, were obtained 288 converted colors for each observer (3 transformations  $\times$  2 hue combinations  $\times$  2 conversions  $\times$  24 color patches). The color patches before and after the transformations were measured with the CS-2000 Spectroradiometer from Konica Minolta (Minolta, 2022), in the same viewing environment in which the psychophysical experiments were conducted (section 3.2).

To perform the measurements, we first displayed the ColorChecker patches in the three different designed profiles to quantify the color difference between the reference and user display before and after the transformations (Figure 4.2). Next, one hue combination was selected (RGBY or RGBO). Once the combination

was set, one of the two conversions was chosen. With the hue set and conversion selected, the three matrix-based transformations were computed and applied to the ColorChecker. Then the result was measured. This procedure was performed for the two hue sets and the two conversions. This workflow can be visualized in the Figure 4.3.

### 4.2.1 Hues combinations

Since the hue data is used to characterize the color properties of the display device, it is possible to choose between different hue combinations to conduct the visual judgments. For example, a set of red, green and blue; red, green, and yellow; or red, green, blue and yellow. The number of implemented hues has to be limited, considering the time to collect the data can be exhausting ( $\sim 15$  minutes for four hues [section 3.2]).

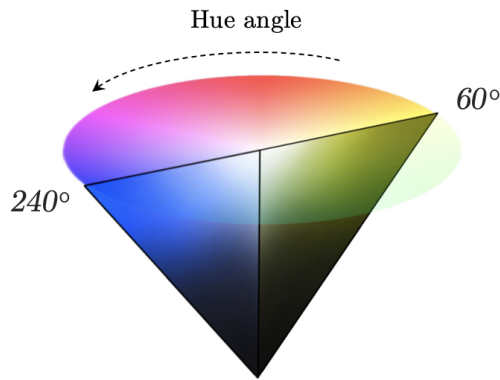


**Figure 4.4:** Visualization of the yellow-blue hue plane in the HSV color space.

In their study, Karatzas and Wuerger (2007) selected the four unique hues (red, green, blue and yellow) to perform their calibration method. They choose these four hues under the assumption that unique hues are constant across human vision. Note that the blue and yellow hues lie on the same plane (Figure 4.4). Then, including the yellow hue to a red, green, and blue combination, the result is a better estimation of the yellow-blue plane (Wuerger, 2008), but in this way, no new plane information is added.

Based on subsequent studies that support no phenomenological difference between unique and binary hues (subsection 3.4.1), and to include a hue that adds information about a new plane, we added a binary hue to one of the two designed sets. Therefore, to conduct our calibration experiments, we used the following sets

of hues: red, green, blue and yellow (RGBY); and red, green, blue and orange (RGBO), (More information on why this orange hue was chosen in subsection 3.4.1). In the last set, all the hues are linearly unrelated.

## 4.2.2 Designed profiles

To fully control the displayed colors in the experiments, we designed three different profiles using the software ColorNavigator 7 to calibrate the Eizo LCD monitor. The built-in sensor was set to calibrate the display automatically.

The three profiles were created using the specifications of the standard sRGB (Table 2.1) but shifting the hue and white point. This way, we can make an analysis purely focused on hue changes without considering other factors that affect the color of the display—for example, different physical properties, gamma value, or brightness. The white shift was introduced to study the performance of the proposed based-matrix transformation that aims to preserve the white point (section 4.5).

**Table 4.1:** Designed profiles white point and hue specifications.

	White point (RGB percentage)	Hues shift (degrees)
Profile 1	(100, 90.45, 73.16)—sRGB	0
Profile 2	(100, 90.45, 73.16)—sRGB	+ 16
Profile 3	(100, 48.28, 30.07)	– 16

The first profile (Profile 1) was as the standard sRGB; the white point and hues were retained. In Profile 2, the white point was preserved as sRGB, but the hues were shifted 16 degrees counterclockwise. In the third, Profile 3, the white point was moved towards the red hues, and the hues were shifted 16 degrees clockwise. The Table 4.1 shows the white point and hue changes for each profile.

It is relevant to clarify that this additional calibration is not part of the calibration method, and its purpose is to control the color behavior of the LCD display for the experiments. These three profiles are assumed to be independent displays.

### 4.2.3 Conversions

The calibration method was applied to do the conversion between two pairs of simulated uncalibrated displays. For this purpose, the three created profiles (subsection 4.2.2) were applied to the same display at different stages. Thus, after applying each profile, the monitor can be assumed as an independent display with the same physical properties but different color behaviors. We can refer to each profile as Display 1, Display 2, and Display 3.

In our experiments, we performed two color conversions: from Display 1 to Display 2, and from Display 1 to Display 3 (Figure 4.5). Thus, with the first conversion, the colors shown on Display 1 were modified to match the colors on Display 2. Whereas after the second conversion, the colors shown on Display 1 should match those displayed on Display 3. In both conversions, Display 1 acts as the user display, and Display 2 and Display 3 are the reference display.

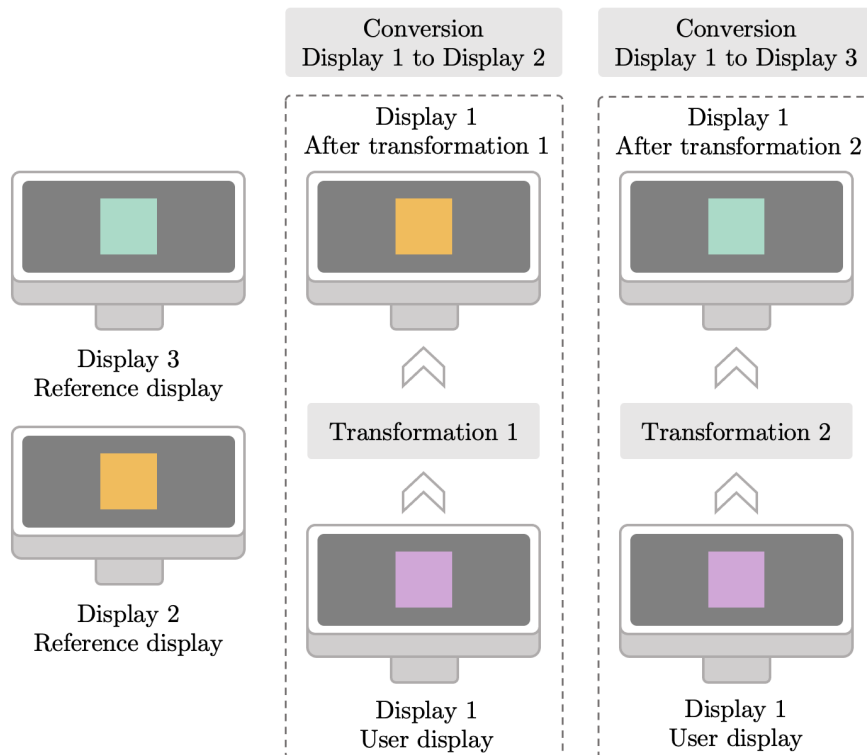


**Figure 4.5:** Two conversions are computed. First, from Display 1 to Display 2. Second, from Display 1 to Display 3.

## 4.3 Display Characterization

To perform calibration, it is fundamental to compute the color conversion between displays in a device-independent color space, since the RGB device-dependent values (digital inputs) do not represent the output color appearance of the display. The mathematical relationship between the input voltage and the light intensity output is given by Equation 2.1. Knowing the parameters of this equation is possible to change the device-dependent RGB values into linear device-dependent RGB. The linear RGB color space is linearly related to XYZ, which is device-independent (subsection 2.3.3). Then, the RGB values are changed into linear RGB before computing the color transformations between two displays, and before applying the transformation to the user display. All the transformation operations are computed in the linear RGB space (Figure 4.6).

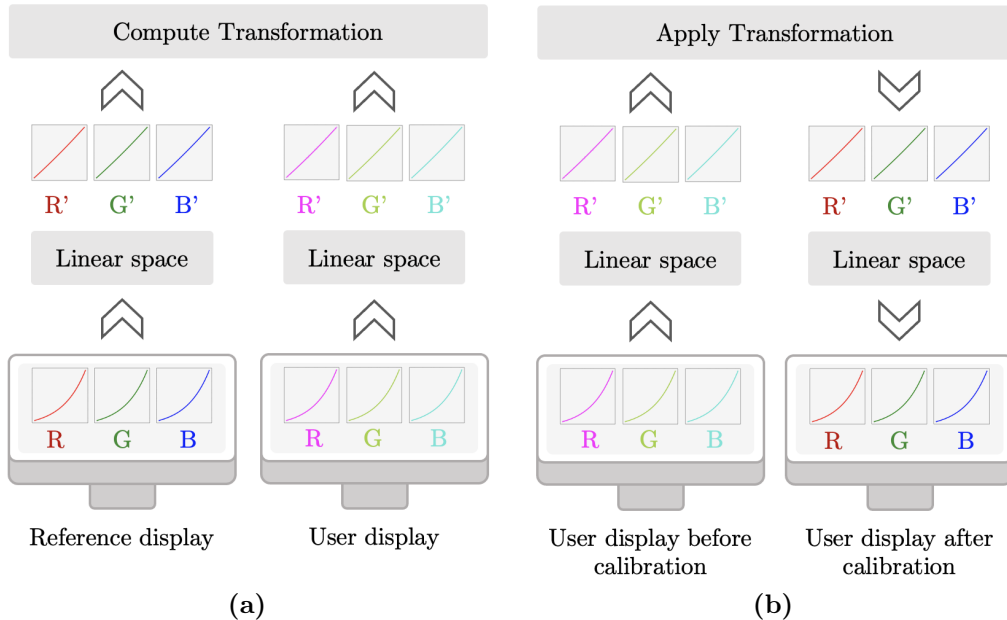


**Figure 4.6:** a) Before computing the color transformation with the user and reference display information, the RGB device-dependent values are converted to the linear RGB space. b) To apply the transformation in the user display, the RGB values also have to be in the linear RGB space.

Because our method aims to eliminate the need for an external standard (e.g., a measuring instrument or a physical color chart), for the calibration used in this project is possible two choose between two approaches: visual approaches or estimation of the signal-to-light-intensity function parameters. Concerning visual approaches, there are several techniques to estimate the *gamma*, *offset*

and *gain* parameters (To et al., 2013) (Ban and Yamamoto, 2013) (Parraga et al., 2014) (Hainich and Bimber, 2016). For example, Ban and Yamamoto (2013) provide an open source calibration software available in (Ban and Yamamoto, 2021), respectively. As a different approach alternative, Wuerger (2008) describes a method to estimate these parameters assuming the unique hues can describe independent planes in the non-linear RGB space.

$$a_{\bar{R}}(g \cdot R + f)^\gamma + b_{\bar{R}}(g \cdot G + f)^\gamma + c_{\bar{R}}(g \cdot B + f)^\gamma + d_{\bar{R}} = 0, \quad (4.1)$$

$$a_{\bar{G}}(g \cdot R + f)^\gamma + b_{\bar{G}}(g \cdot G + f)^\gamma + c_{\bar{G}}(g \cdot B + f)^\gamma + d_{\bar{G}} = 0, \quad (4.2)$$

$$a_{\bar{B}}(g \cdot R + f)^\gamma + b_{\bar{B}}(g \cdot G + f)^\gamma + c_{\bar{B}}(g \cdot B + f)^\gamma + d_{\bar{B}} = 0. \quad (4.3)$$

where  $g$  is the *gain*,  $f$  is the *offset*, and  $\gamma$  is the gamma. The vector  $[a_i, b_i, c_i]$  is the normal of the plane.  $R$ ,  $G$  and  $B$  are the red, green and blue pixel value coordinates.

The collected hue data can be used to define the normal of the hue planes ( $[a_i, b_i, c_i]$ ). Then, utilizing different points (RGB) from the same hue plane (e.g. Saturation-Value combinations in the HSV color space from the data hue collection), and applying Equation 2.1, is possible to estimate the *gamma*, *offset* and *gain* values. Finally, the estimation can be computed through a standard minimisation procedure (Wuerger, 2008), using the equations Equation 4.1, Equation 4.2, and Equation 4.3 for each hue plane.

The approaches discussed above are the characterization alternatives independent of an external standard. However, in our experiments, we did not apply these characterization approaches. The display we used was calibrated in sRGB. Thus we directly applied Equation 2.2 to make the transformations between device-dependent RGB and linear device-dependent RGB.

## 4.4 Display Profile

The hue judgments data is used to create the display profile, which characterizes its color behavior. After the hue data collection, a specific device profile is created. This profile is a file that contains the necessary information to compute the transformation matrix used to calibrate a display, such as the collected hue coordinates in RGB color space and the signal-to-light-intensity function.

Depending on the used matrix-based transformation method (section 4.5), the display profile can also include the normal vectors computed from each hue plane in the linear device-dependent RGB space. During the hue collection experiments,

the same set of hues (e.g. red hues, green hues or blue hues) were shown at different levels of saturation and value (More information about the points we selected on the plane in section 3.4). Then, each set of visual hue judgments can be fitted to form a plane in the linear RGB space (Karatzas and Wuerger, 2007) (Figure 4.7). From the hue plane equation is calculated the normal vector that defines its orientation in the three-dimensional space.

To fit a set of hue coordinates into a plane, we implemented a function by Leygue (2022) which minimizes the sum of the quadratic distances between the 3D points and the predicted plane. This fitting is computed by using the eigenvalues associated with the points distribution.

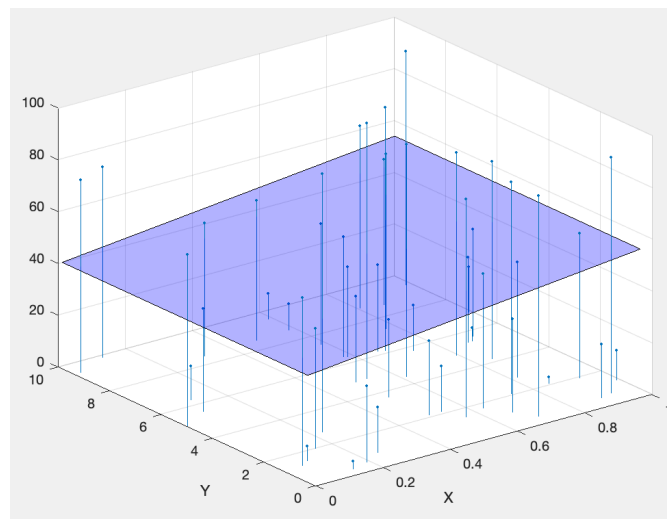


**Figure 4.7:** Visualization of 3D points fitting into a plane. The points represent the RGB selected coordinates of a hue set, and the plane would be the correspondent hue plane.

## 4.5 Matrix-Based transformations

The vector bases of the linear user-RGB and linear reference-RGB spaces are linearly related (Karatzas and Wuerger, 2007). Then, a matrix can be applied to transform the linear user-RGB coordinates into the linear reference-RGB ones. In this project, the matrix-based transformations are computed using the information contained in two display profiles, one from the user and the other from the reference displays. Next, this transformation is applied to adjust the linear RGB values from the user display to match the reference color appearance.

In order to conduct our calibration experiments, we computed three different transformations, which are explained below.

### 4.5.1 Point to Point Transformation

The purpose of the point-to-point matrix-based transformation is to convert the linear RGB coordinates from the user display (linear user-RGB) into the linear RGB coordinates of the reference display (linear reference-RGB). It is a point-to-point transformation. Compared with transformations that need a characterized hue plane (e.g, subsection 4.5.2), the computation of a Point-to-Point matrix is not limited by a number of coordinates to define the plane equation of a single hue. Thus, it could result in less assessments and include a wide variety of hues.

We computed an unconstrained nonlinear optimization in the linear RGB space to estimate the matrix that performs the point-to-point transformation. The optimization finds the minimum of an unconstrained multivariable function using a derivative-free method. The objective function (Equation 4.4) was set as the Root-Mean-Square Error (*RMSE*) (Equation 4.5) between the predicted linear user-RGB after the transformation and the linear reference-RGB.

$$\begin{bmatrix} r^{lin} \\ g^{lin} \\ b^{lin} \end{bmatrix}_{pre,user}^T = \begin{bmatrix} r^{lin} \\ g^{lin} \\ b^{lin} \end{bmatrix}_{user}^T \cdot \begin{bmatrix} t_{11} & t_{12} & t_{13} \\ t_{21} & t_{22} & t_{23} \\ t_{31} & t_{32} & t_{33} \end{bmatrix} \quad (4.4)$$

where *pre, user* vector is the predicted linear user-RGB and *user* vector is the actual user-RGB collected from one point of the hue data.  $t_{ij}$  are the elements of the point-to-point matrix-based transformation.

$$RMSE = \sqrt{\frac{1}{n} \sum_{i=1}^n (x_i - \hat{x}_i)^2} \quad (4.5)$$

where  $n$  is the number of data points,  $x_i$  the actual data value,  $\hat{x}_i$  the predicted data value, and  $i$  is the data index.

Before inputting the data to minimize the objective function, we changed the hue judgment data into their symmetrical angle with respect to the expected hue angle in the HSV color space (Equation 4.6).

$$\phi = \beta + (\beta - \alpha) \quad (4.6)$$

where  $\phi$  is the symmetrical hue angle of  $\alpha$  with respect to the  $\beta$  angle.

A way of mapping the selected hue points in the user and reference displays is to consider the color appearance of the displayed colors in both displays. When

an observer selects a hue patch as pure, this visual judgment defines the relation between the RGB values and its visual appearance. For example, if a magenta-red (in the view of the reference display) is selected as pure red in the user display, it means that the user display is shifting the red hues towards the yellow angle. A pure red would be expected to be  $0^\circ$  in HSV for a calibrated display (e.g., sRGB color space).

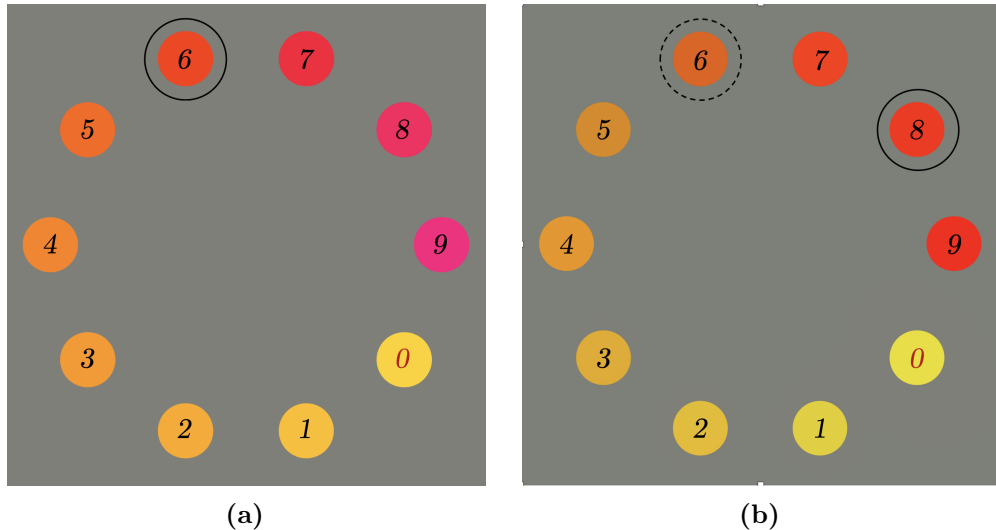


**Figure 4.8:** Example of a hue selection. a) patch number 6 is selected as pure red for a calibrated display. b) patch number 8 is selected as pure red for an uncalibrated display. Patch number 6 has a yellowish-red color appearance for this case of uncalibrated display, then the patch that appears as pure red is shifted to patch number 8.

#### 4.5.2 Point to Plane Transformation

The point-to-plane transformation was implemented following the study by Karatzas and Wuergler (2007). This transformation maps the linear reference-RGB points into their correspondent hue planes in the linear user-RGB space. To this end, the point-to-point transformation is obtained by minimizing the distance between the linear reference-RGB points and the hue planes in the linear user-RGB space (Equation 4.7). To solve the minimization problem, a constrained optimization was employed where the objective function was the RMSE of the distance between the transformed linear reference-RGB and the linear user-RGB planes. We computed the constrained nonlinear optimization using the gradient based method provided

by the MATLAB function *fmincon*.

$$\begin{bmatrix} r_h^{lin} & g_h^{lin} & b_h^{lin} \end{bmatrix}_{ref} \cdot \begin{bmatrix} t_{11} & t_{12} & t_{13} \\ t_{21} & t_{22} & t_{23} \\ t_{31} & t_{32} & t_{33} \end{bmatrix} \cdot \begin{bmatrix} \alpha_h^{lin} \\ \beta_h^{lin} \\ \gamma_h^{lin} \end{bmatrix}_{user} = 0 \quad (4.7)$$

were the array  $[r_h^{lin} \ g_h^{lin} \ b_h^{lin}]_{ref}$  describes the hue point coordinates in the three-dimensional space for the reference display, and the array  $[\alpha_h^{lin} \ \beta_h^{lin} \ \gamma_h^{lin}]^T_{user}$  specifies the normal vector of the user plane.  $T$  is the point-to-plane  $3 \times 3$  transformation matrix.

The previous linear system is solved using as input the set of hue points from the reference display and the computed corresponding planes from the user display. Since there are different ways to map a point into a plane (e.g., referring to the rotation or scaling of the data set) (Karatzas and Wuenger, 2007), and therefore different solutions for the Equation 4.7, two constraints are included in the optimization. First, the sum of elements in each row of the transformation matrix is set to be 1 (Equation 4.8); in the second constrain, the highest saturation in the set of hue points was preserved after the transformation (Equation 4.9).

$$t_{11} + t_{12} + t_{13} = 1; t_{21} + t_{22} + t_{23} = 1; t_{31} + t_{32} + t_{33} = 1. \quad (4.8)$$

$$\begin{bmatrix} r^{lin} \\ g^{lin} \\ b^{lin} \end{bmatrix}_{ref}^T = \begin{bmatrix} r^{lin} \\ g^{lin} \\ b^{lin} \end{bmatrix}_{ref}^T \cdot \begin{bmatrix} t_{11} & 0 & 0 \\ 0 & t_{22} & 0 \\ 0 & 0 & t_{33} \end{bmatrix} \quad (4.9)$$

where  $t_{ij}$  are the elements of the point-to-plain transformation, and  $[r^{lin} \ g^{lin} \ b^{lin}]_{ref}$  the linear reference-RGB data points.

### 4.5.3 White Preservation Transformation

The chromaticity of the gray scale is essential in color vision. The human visual system perceives color relative to a white reference. Changes in the white chromaticities have a huge impact on the appearance of the surrounding colors (Elliot et al., 2015). For this reason, we decided to implement an additional constraint whose purpose is to preserve the grey scale after applying the matrix-based transformation. This matrix-based transformation follows the previous one (subsection 4.5.2), were the coordinates are mapped to a plane.

Since the neutral gray of the display was previously recorded from the data collection stage, it was used for calculating the constrained transformation (White preservation transformation). Even though we called it "preservation," the constraint

implies that the neutral gray selected from the reference display was transformed into the user neutral grey. Equation 4.10 shows the implemented condition.

$$\begin{bmatrix} r^{lin} \\ g^{lin} \\ b^{lin} \end{bmatrix}_{ref,grey}^T = \begin{bmatrix} r^{lin} \\ g^{lin} \\ b^{lin} \end{bmatrix}_{user,grey}^T \cdot \begin{bmatrix} t_{11} & t_{12} & t_{13} \\ t_{21} & t_{22} & t_{23} \\ t_{31} & t_{32} & t_{33} \end{bmatrix} \quad (4.10)$$

where the *ref, grey* array describes the linear RGB values of the selected neutral grey on the reference display, and *user, grey* is the selected linear RGB on the user display.  $t_{ij}$  are the elements of the White preservation transformation.

## 4.6 Evaluation of Calibration

To evaluate the calibration method, we first applied the matrix-based transformations to the linear RGB values of the ColorChecker patches (Equation 4.11, Equation 4.12). The result was displayed and measured. Using the measurements from the user display, after the transformations, and the reference display, the CIE 2000 color difference (*CIEDE2000*  $\Delta E_{00}$ ) (Luo et al., 2001) formula was computed.

$$[r^{lin} \quad g^{lin} \quad b^{lin}]_{user} = [r^{lin} \quad g^{lin} \quad b^{lin}]_{ref} \cdot T \quad (4.11)$$

$$\begin{bmatrix} r^{lin} \\ g^{lin} \\ b^{lin} \end{bmatrix}_{user}^T = \begin{bmatrix} r^{lin} \\ g^{lin} \\ b^{lin} \end{bmatrix}_{ref}^T \cdot \begin{bmatrix} t_{11} & t_{12} & t_{13} \\ t_{21} & t_{22} & t_{23} \\ t_{31} & t_{32} & t_{33} \end{bmatrix} \quad (4.12)$$

where the *user* vector are the linear user-RGB, the *ref* vector are the linear reference-RGB, and *T* is the matrix-based transformation.

For each of the two conversions, three matrices were applied per subject (3 matrices  $\times$  6 observers). For each observer, they perform the hue judgments in each display. Thus, the user profile and display reference were used to obtain the transformations. Then, to quantify the color differences were first calculated, the  $\Delta E_{00}$  between the displayed ColorChecker patches in Display 1 and Display 2. Next, to analyze the color change on Display 1 after the matrix-based transformations, the color difference was computed between the patches measured in the original Display 2 and the patches measured in Display 1 after the matrix-based transformations. In this way, we obtained six values of color differences for each ColorChecker patch, a total of 144 color differences (6 observers  $\times$  24 color patches) for each transformation. For the three transformations, an ideal result would be  $\Delta E_{00} = 0$ , which means that the color appearance of Display 1 after the transformations matches the color appearance of Display 2.

# 5 | Results and Discussion

This chapter presents and discusses the results obtained from the previous experiments.

## 5.1 From Display 1 to Display 2

Figure 5.2, Figure 5.3, and Figure 5.4 show the results in terms of color difference ( $\Delta E_{00}$ ) of each patch of the ColorCheker when the direction of the conversion is from Display 1 to Display 2.

### 5.1.1 Color differences per ColorChecker patch

Figure 5.2a, Figure 5.3a, and Figure 5.4a present the averaged  $\Delta E_{00}$  values from all the 6 observers and for each ColorChecker patch. The colored bars correspond with the results from the Point-to-Point transformation; the upper blue bars are the color differences before applying the transformation.



**Figure 5.1:** ColorCheker used to test the matrix-based transformations performance.

The Point-to-Point transformation (Figure 5.2a) reduces the color difference for the red hues, such as red and moderate red patches. For the yellow-red and red-purple hues (Munsell color system), such as dark skin, light skin, orange-yellow, orange, and magenta, the average results are similar compared to before

## Chapter 5 | RESULTS AND DISCUSSION

the transformation. The color differences on the rest of the patches show a bad performance of the transformation, especially on the greyscale patches.

The Point-to-Plane transformation (Figure 5.3a) also reduces the color difference for the red patches. Moreover, in this case, the color difference on the yellow patch is decreased as well. Therefore, the results are improved for the red-yellow hues (Munsell color system) compared to the original displays difference, and to the Point-to-Point transformation.

The color differences obtained from the White transformation (Figure 5.4a) for the yellow and green hue patches are similar to those obtained from the Point-to-Plane transformation. Thus, the green and yellow hue mixtures. However, this matrix significantly increases the color differences for the red and green patches, such as blue sky, moderate red, blue, red, or magenta.

Including the results from the three matrix-based transformations, the patches that show an improvement are the colors that presented the largest color difference between Display 1 and Display 2. For example, in the red, moderate red, and orange patches of the ColorChecker. However, the differences for the remaining patches are increased, particularly on the greyscale.

### 5.1.2 Color differences per Observer

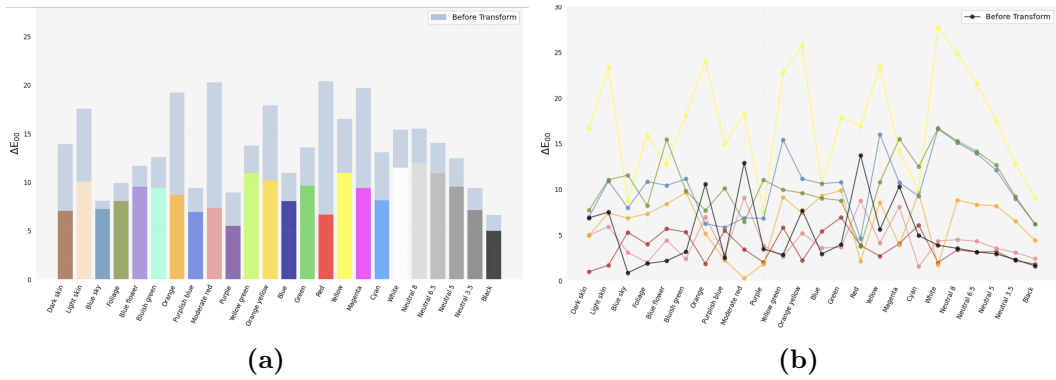
Even though using the average color difference of each patch is possible to visualize in a general way the performance of the matrix-based transformations, it is important to take into account how it varies between observers. The calibration method should apply to any observer.

Figure 5.2b, Figure 5.3b, and Figure 5.4b show the color differences obtained from each observer. The black line of the Figures represents the original Display 1-Display 2 color differences. Each of the colored lines show the performance of an individual transformation for each observer (transformation calculated from the data of each observer individually).

There is some interesting information we could get from these results. First, comparing the results of the three transformations, the Point-to-Point matrix produces inconsistent results between observers. However, note that this transformation does not apply any constrain. Moreover, the Point-to-Point mean color difference is not significantly large compared to the other transformations (see Table 5.1); 1.65 and 0.22 difference from the Point-to-Plane and White preservation transformations, respectively, where 1 unit is the Just Noticeable Difference (JND). Further work would be necessary to test the matrix performance under constraints.

Comparing the Point-to-Point (Figure 5.3b) and White preservation transformations (Figure 5.4b), it is observed that applying the White preservation transform

makes the results more consistent among observers. Figure 5.4b shows two distinct groups: red, pink, and orange lines (first group); and blue, green, and yellow lines (second group). For the three transformations is repeated that the first group obtains better performance than the second group. In the first group, for the White transformation (Figure 5.4b), the color differences for the dark skin, light skin, orange, moderate red, yellow-green, red, yellow, and magenta patches are decreased. Moreover, the greyscale is preserved. Differently, the second group only reduce the color difference in two patches, orange and red. When relating the data responses to the information from the observer, it is found that the first group includes people whose field of work is color science. These results suggest that previous knowledge in color science could influence the results. To study this phenomenon, the data from a larger number of observers and the difference between their individual hue responses would be required.



**Figure 5.2:** From Display 1 to Display 2. a) Mean  $\Delta E_{00}$  of six observers for each ColorCheker patch. The upper blue bars are the original color differences. The colored bars are the color differences after the Point-to-Point transformation. b)  $\Delta E_{00}$  per observer. The black line shows the original  $\Delta E_{00}$  values. Each colored line corresponds with the color differences for one observer.

## 5.2 From Display 1 to Display 3

Figure 5.5, Figure 5.6, and Figure 5.7 show the color differences ( $\Delta E_{00}$ ) results from each measured patch of the ColorCheker when the direction of the conversion is from Display 1 to Display 3.

The difference between Display 2 and Display 3 is that the second one shifts the hues in a symmetric angle (HSV color space), and the white point is modified to be reddish (Table 4.1).

## Chapter 5 | RESULTS AND DISCUSSION

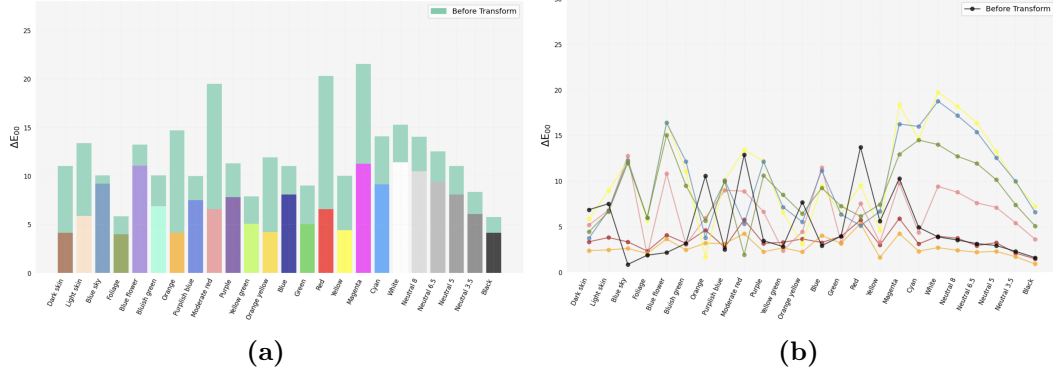


**Figure 5.3:** From Display 1 to Display 2. a) Mean  $\Delta E_{00}$  of six observers for each ColorCheker patch. The upper blue bars are the original color differences. The colored bars are the color differences after the Point-to-Plane transformation. b)  $\Delta E_{00}$  per observer. The black line shows the original  $\Delta E_{00}$  values. Each colored line corresponds with the color differences for one observer.

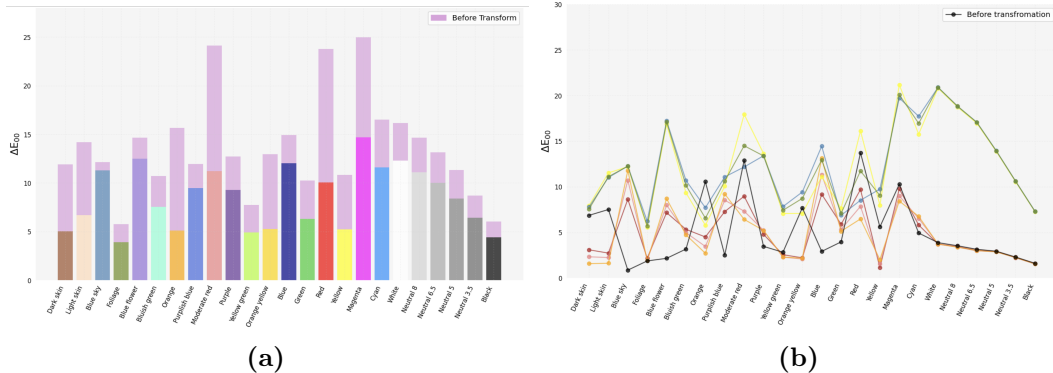


**Figure 5.4:** From Display 1 to Display 2. a) Mean  $\Delta E_{00}$  of six observers for each ColorCheker patch. The upper blue bars are the original color differences. The colored bars are the color differences after the White preservation transformation. b)  $\Delta E_{00}$  per observer. The black line shows the original  $\Delta E_{00}$  values. Each colored line corresponds with the color differences for one observer.

### 5.2.1 Color differences per ColorChecker patch

Figure 5.5a, Figure 5.6a and Figure 5.7a show that in this case of conversion, the transformations do not perform well for any particular group of hues. After the transformations, the averaged color difference results are close to the original difference. However, it can be noted that the White preservation transformation (Figure 5.4a) reduces the  $\Delta E_{00}$  for the greyscale. Even though it increases the color differences of other color patches, such as cyan, the greyscale preservation could mean an improvement in terms of color appearance due to the importance of the white point.

### 5.2.2 Color differences per Observer

Looking at Figure 5.5b, Figure 5.6b and Figure 5.7b is visible that there is exist more consistency between observers compared with the previous conversion (Display 1 to Display 2). These results support the previous observation where two groups of observers can be distinguished. For the three matrix-based transformations, two groups are divided by the black line that shows the original color difference between Display 1 and Display 3. This means that for most of the patches in the three matrices, the transformations improve the color difference between displays for the three grouped observers.

If we analyze the White preservation for the first group in Figure 5.7b, it appears more patent the color difference improvement of the greyscale, thus the light color patches, such as light skin, blue sky, or bluish green. Considering the similar behavior between observers, for this particular conversion, the White preservation transformation performs the best (Figure 5.4a).

**Table 5.1:** Mean and STD of  $\Delta E_{00}$  for the three matrix-based transformation used in the conversion from Display 1 (D1) to Display 2 (D2), and from Display 1 to Display 3 (D3).

$(\Delta E_{00})$	T Point-to-Point		T Point-to-Plane		T Grey scale	
Conversions	Mean	STD	Mean	STD	Mean	STD
D1 to D2	8.7353	5.1550	7.1126	3.4728	8.5330	3.7914
D1 to D3	20.9393	4.4262	19.04475	5.5264	18.3841	5.1555

## Chapter 5 | RESULTS AND DISCUSSION

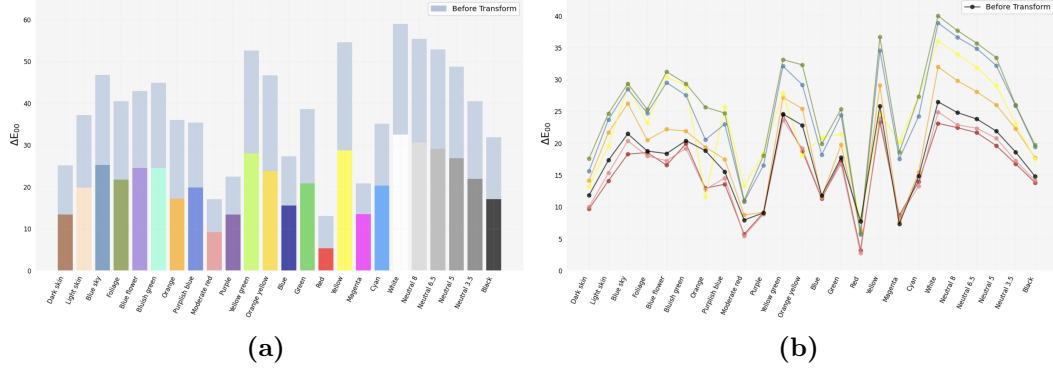


**Figure 5.5:** From Display 1 to Display 3. a) Mean  $\Delta E_{00}$  of six observers for each ColorCheker patch. The upper blue bars are the original color differences. The colored bars are the color differences after the Point-to-Point transformation. b)  $\Delta E_{00}$  per observer. The black line shows the original  $\Delta E_{00}$  values. Each colored line corresponds with the color differences for one observer.

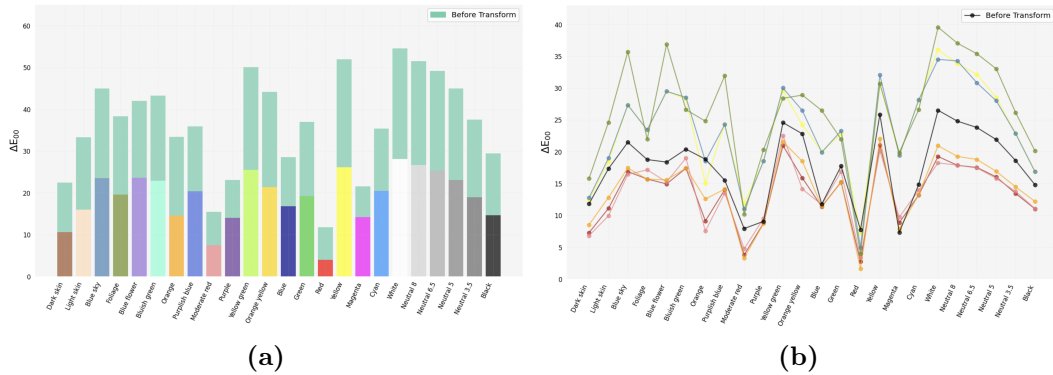


**Figure 5.6:** From Display 1 to Display 3. a) Mean  $\Delta E_{00}$  of six observers for each ColorCheker patch. The upper blue bars are the original color differences. The colored bars are the color differences after the Point-to-Plane transformation. b)  $\Delta E_{00}$  per observer. The black line shows the original  $\Delta E_{00}$  values. Each colored line corresponds with the color differences for one observer.

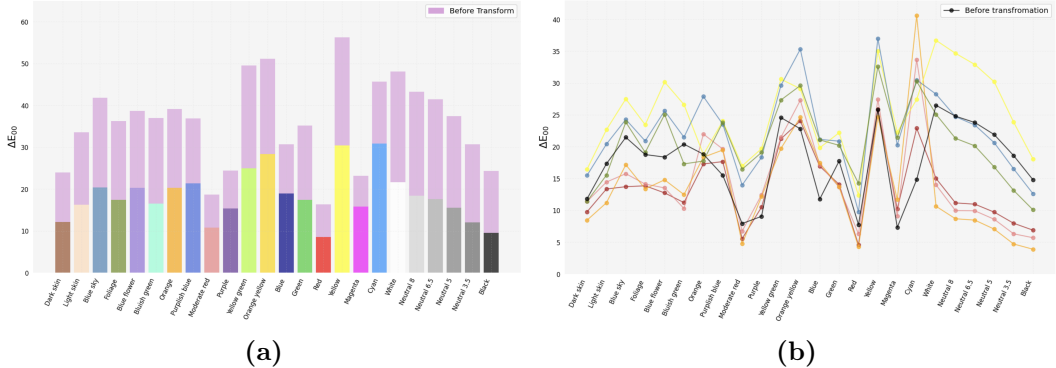


**Figure 5.7:** From Display 1 to Display 3. a) Mean  $\Delta E_{00}$  of six observers for each ColorCheker patch. The upper blue bars are the original color differences. The colored bars are the color differences after the White preservation transformation. b)  $\Delta E_{00}$  per observer. The black line shows the original  $\Delta E_{00}$  values. Each colored line corresponds with the color differences for one observer.

## 5.3 Hue combinations

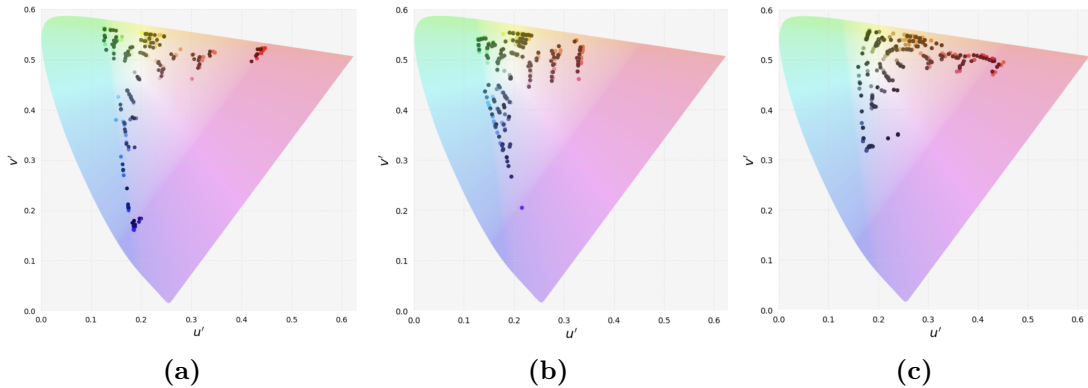
Figure 5.10 illustrates the averaged  $\Delta E_{00}$  for the two sets of hues: red, green, blue, and yellow; and red, green, blue, and orange. The three transformations show similar performance for both sets of hues. The largest difference is in the second conversion, for the Point-to-Plane and White preservation, where the  $\Delta E_{00}$  is approximately 1 JND.

Figure 5.8 and Figure 5.9 present the color choices of the 13 observers in the CIE 1976 chromaticity diagram. For the three displays (Figure 5.9a, Figure 5.9b and Figure 5.9c), the orange hue selections are less variable between observers compared with other hues, for example, the red answers. On the other hand, in Display 3, the orange hue overlaps the red selections Figure 5.9c; this could be related to the decrease in performance that shows Figure 5.10 for the hue set that includes the orange hue, in the second conversion. To correctly sample the three-dimensional color space, the hue planes should be equally distributed, providing information to map all color combinations. If two hue planes are spatially close, it will be similar to employing three hue planes instead of four, thus having less color information to compute the matrix transformation.

A balance between the inter-observer variability and the transformation performance for a specific set of hues is needed. For our experiments, replacing a unique hue with a binary hue result in a 1.2  $\Delta E_{00}$  increase (averaged result). However, a reduction in the observer inter-variability could compensate for this disadvantage. Moreover, it would also be interesting to study other hue planes that are more distant, in terms of color appearance, from the unique hues and, therefore, hard to

## Chapter 5 | RESULTS AND DISCUSSION

overlap hue responses.



**Figure 5.8:** Unique hue selections over the CIE 1976 Chromaticity Diagram (The euclidean distance between two points quantifies their color differences). a) Display 1 (sRGB calibrated). b) Display 2. b) Display 3.

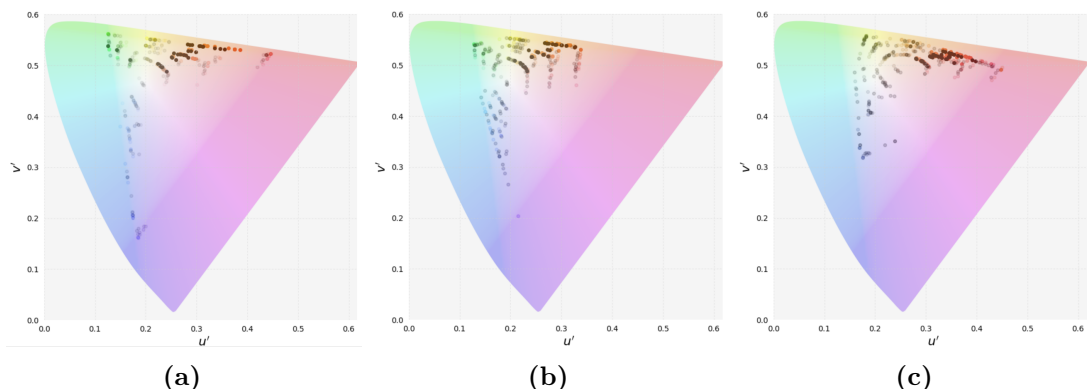


**Figure 5.9:** Orange hue selections over the CIE 1976 Chromaticity Diagram (The euclidean distance between two points quantifies their color differences). a) Display 1 (sRGB calibrated). b) Display 2. b) Display 3.

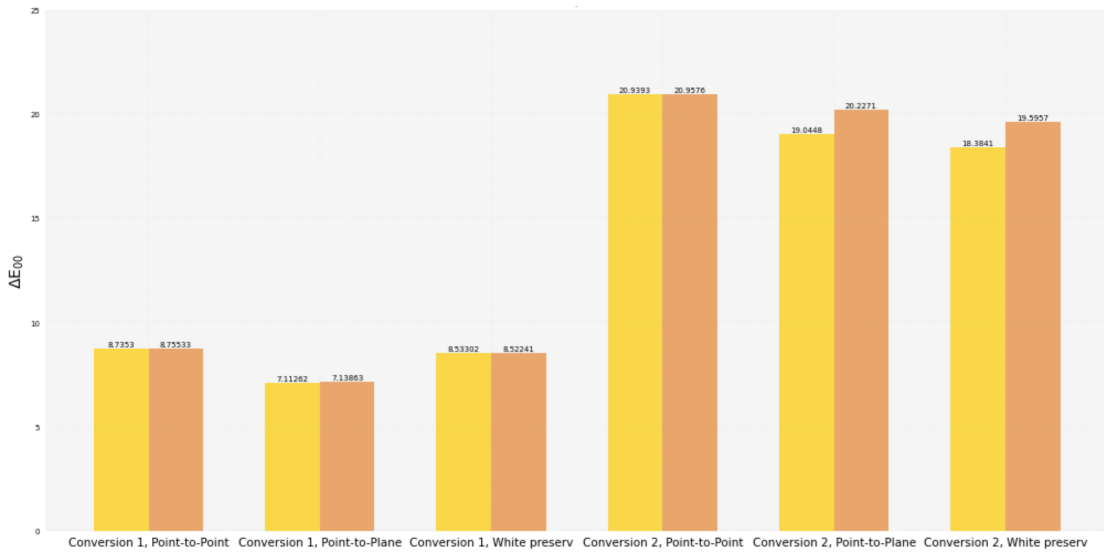


**Figure 5.10:** red, green, yellow, and blue set (yellow bars) compared against red, green, yellow, and orange set (orange bars). The first three pair of bars shows the averaged  $\Delta E_{00}$  for the first conversion. The second three pair of bars shows the averaged results in the second conversion. The transformations are Point-to-Point, Point-to-Plane, and White preservation, in that order.

# 6 | Conclusions

## 6.1 Summary

This project applies the visual calibration method proposed by Karatzas and Wuerger (2007), which is based on visual judgments and does not require a measurement device. The aim is to communicate accurate color between display devices remotely.

To perform the calibration method, we implemented a user interface that we designed in JavaScript to conduct psychophysical experiments. The subjects were instructed to select colors among a displayed annulus of stimuli. The task was to select pure hues, e.g., a color such that neither red nor green appeared. The experiments derived a display profile that stores its color properties.

Given two display profiles, from a reference and a target display, we computed the transformation that adjusts the color of the target display to match the reference. This transformation was applied to do the conversion between two pairs of displays.

To perform the conversions, we computed three different matrix-based transformations, two of which we first proposed. The first matrix maps the color coordinates of a reference display to a target display. This matrix shows inconsistent results when the conversion is between displays with small color differences. However, note that it does not apply any constraint, and the resulting averaged difference compared with the other matrices is approximately 1 JND. Applying this transformation would imply advantages, such as including different hues or reducing the number of assessments. The second transformation was implemented using as reference the work by Karatzas and Wuerger (2007), their transformation maps color coordinates to hue planes. For the first conversion, this transformation gives the best results; it also improves the inconsistent results of the previous matrix. Finally, the third matrix also maps coordinates to planes, but in this case, an additional constraint is applied to preserve the grayscale of the display. For screens whose white point chromaticities are distant, we managed to reduce their color difference. These results are promising, given the importance of achromatic stimuli on the perception of surrounding colors.

We observed two differentiated groups of observers from the color differences obtained after the conversions. For the first group, the transformations improve the original color differences between the displays. However, for the second group of observers, the color differences increased after the transformations. The field of work of the first group is color science. In contrast, the second group is color-unrelated, suggesting that prior knowledge in color science can significantly impact the calibration method.

Finally, the transformations applied to two hue combinations were also studied. The first one includes two four unique hues, and the second one replaces the yellow of the first set with a binary hue, which is orange. The set of hues, including orange, obtained the same results in the first conversion as the unique hue set. However, for the second conversion, the results get worse. As a possible explanation, we could see in the hue selections that the orange responses overlap the red. Thus the three-dimensional color space might not be properly sampled.

That similar results are obtained opens the option of including binary hues with a reduced inter-observer variability or hues that define a plane spatially more distant from the other hue planes, so the color mapping between displays could increase in accuracy.

## 6.2 Future Work

Given the lack of time, future work is required, which could first focus on the analysis of the data collected. From the hue judgments, we could analyze the individual variations between observers and how these affect the calibration process. Also, apply metrics that quantify this factor. Concerning the calculated color differences after the conversion, it is necessary to analyze them more in detail by providing a larger amount of numerical data, such as other color differences formulas like CIE  $L^*C^*h$ , in which the differences in hue can be isolated. Moreover, include more observers of the hue collection experiment to provide more reliable results. On the other hand, it would also be interesting to study the neutral gray responses selected for the three types of profiles.

Since we also collected the time taken by each observer to select each hue, it would be relevant to study how this factor affects the results. Also, to design a method that includes the fastest choices and produces less eye fatigue.

The next step would be to perform psychophysical experiments to test the transformations applied in real images. Even though  $\Delta E$  is a good starting point to quantify color differences, it is not enough in a real-world context. In images, we should consider other factors such as the complexity of the scene or properties like size or texture. For example, color differences are less perceptible in complex scenes. Other visual processes such as color memory can also influence the color evaluation (Sharma, 2018). Therefore, judging the color difference between several transformed images is essential. The human criteria will give a more appropriate evaluation of how the calibration is performing.

# Bibliography

- Amani, M., Falk, H., Jensen, O. D., Vartdal, G., Aune, A., and Lindseth, F. (2019). Color calibration on human skin images. In *International Conference on Computer Vision Systems*, pages 211–223. Springer. (cited on page 21)
- Anstis, S. and Cavanagh, P. (1983). *A minimum motion technique for judging equiluminance*. York University. (cited on page 22)
- Arstila, V. (2018). What makes unique hues unique? *Synthese*, 195(5):1849–1872. (cited on page 31)
- Ban, H. and Yamamoto, H. (2013). A non-device-specific approach to display characterization based on linear, nonlinear, and hybrid search algorithms. *Journal of Vision*, 13(6):20–20. (cited on pages 22 and 41)
- Ban, H. and Yamamoto, H. (2021). Hsv and hsl (colorpsaces xi). <https://github.com/hiroshiban/Mcalibrator2>. Accessed: 2022-08-05. (cited on page 41)
- Bao, W., Wei, M., and Xiao, K. (2020). Investigating unique hues at different chroma levels with a smaller hue angle step. *JOSA A*, 37(4):671–679. (cited on page 3)
- Barnard, K. and Funt, B. (2002). Camera characterization for color research. *Color Research & Application: Endorsed by Inter-Society Color Council, The Colour Group (Great Britain), Canadian Society for Color, Color Science Association of Japan, Dutch Society for the Study of Color, The Swedish Colour Centre Foundation, Colour Society of Australia, Centre Français de la Couleur*, 27(3):152–163. (cited on page 20)
- Bosten, J. and Boehm, A. (2014). Empirical evidence for unique hues? *JOSA A*, 31(4):A385–A393. (cited on pages 29 and 31)
- Bosten, J. and Lawrance-Owen, A. (2014). No difference in variability of unique hue selections and binary hue selections. *JOSA A*, 31(4):A357–A364. (cited on pages 31 and 32)
- Braun, G. J. (2003). Visual display characterization using flicker photometry techniques. In *Human Vision and Electronic Imaging VIII*, volume 5007, pages 199–209. SPIE. (cited on page 22)
- Castellano, J. A. (2012). Handbook of display technology. (cited on pages 11 and 24)

## BIBLIOGRAPHY

- Chauhan, T., Perales, E., Xiao, K., Hird, E., Karatzas, D., and Wuerger, S. (2014). The achromatic locus: effect of navigation direction in color space. *Journal of vision*, 14(1):25–25. (cited on page 26)
- Cochrane, S. (2014). The munsell color system: A scientific compromise from the world of art. *Studies in History and Philosophy of Science Part A*, 47:26–41. (cited on page 9)
- Consortium, I. C. (2022a). Display calibration. <https://www.color.org/displaycalibration.xalter#custom>. Accessed: 2022-07-26. (cited on pages 16 and 20)
- Consortium, I. C. (2022b). Making color seamless between devices and documents. <https://www.color.org/index.xalter>. Accessed: 2022-07-18. (cited on page 6)
- Consortium, I. C. (May 2008). Wp23: Rgb color managed workflow example. (cited on page 8)
- Consortium, I. C. (Updated Oct 2020). Wp4: Color management overview. (cited on pages 6 and 12)
- Consortium, I. C. et al. (2004). Image technology colour management-architecture, profile format, and data structure. *Specification ICC. 1: 2004-10 (Profile version 4.2. 0.0)*. (cited on pages 7, 20, and 21)
- Eizo (2022). Coloredge cg279x hardware calibration lcd monitor. <https://www.eizo.com/products/coloredge/cg279x/>. Accessed: 2022-08-04. (cited on page 35)
- Elliot, A. J., Fairchild, M. D., and Franklin, A. (2015). *Handbook of color psychology*. Cambridge University Press. (cited on pages 10, 11, 12, 13, 14, 17, and 45)
- Forder, L., Boston, J., He, X., and Franklin, A. (2017). A neural signature of the unique hues. *Scientific reports*, 7(1):1–8. (cited on page 32)
- Fraser, B., Murphy, C., and Bunting, F. (2002). *Real world color management*. Pearson Education. (cited on pages 6, 7, 9, and 18)
- Gerrits, H. and Vendrik, A. (1970). Simultaneous contrast, filling-in process and information processing in man's visual system. *Experimental Brain Research*, 11(4):411–430. (cited on page 26)
- Giorgianni, E. J. and Madden, T. E. (2008). *Digital color management: Encoding solutions*. John Wiley & Sons. (cited on page 21)

## BIBLIOGRAPHY

- Hainich, R. R. and Bimber, O. (2016). *Displays: fundamentals & applications*. AK Peters/CRC Press. (cited on page 41)
- Hering, E. (1964). Outlines of a theory of the light sense. (cited on page 3)
- Hurvich, L. M. and Jameson, D. (1957). An opponent-process theory of color vision. *Psychological review*, 64(6p1):384. (cited on page 26)
- Johnson, T. (1996). *Colour management in graphic arts and publishing*. Pira International. (cited on page 8)
- jsPsych (2022). <https://www.jspsych.org/7.2/>. Accessed: 2022-06-19. (cited on page 23)
- Kahu, S. Y., Raut, R. B., and Bhurchandi, K. M. (2019). Review and evaluation of color spaces for image/video compression. *Color Research & Application*, 44(1):8–33. (cited on page 11)
- Kang, H. R. (2006). *Computational color technology*. Spie Press Bellingham. (cited on page 13)
- Karatzas, D. and Wuergler, S. (2007). A hardware-independent colour calibration technique. *Annals of the BMVA Vol*, 2007(3):1–11. (cited on pages 3, 4, 22, 26, 30, 37, 42, 44, 45, and 56)
- Kay, R. L. and Brandenberg, C. B. (2007). Characterization of the nonlinearities of a display device by adaptive bisection with continuous user refinement. US Patent 7,304,482. (cited on page 22)
- Lago, M. A. (2021). Simplephy: An open-source tool for quick online perception experiments. *Behavior Research Methods*, 53(4):1669–1676. (cited on page 2)
- Leygue, A. (2022). Plane fit. <https://se.mathworks.com/matlabcentral/fileexchange/43305-plane-fit>. Accessed: 2022-08-05. (cited on page 42)
- Luo, M. R., Cui, G., and Rigg, B. (2001). The development of the cie 2000 colour-difference formula: Ciede2000. *Color Research & Application: Endorsed by Inter-Society Color Council, The Colour Group (Great Britain), Canadian Society for Color, Color Science Association of Japan, Dutch Society for the Study of Color, The Swedish Colour Centre Foundation, Colour Society of Australia, Centre Français de la Couleur*, 26(5):340–350. (cited on page 46)
- Matthen, M. (2020). Unique hues and colour experience. In *The Routledge handbook of philosophy of colour*, pages 159–174. Routledge. (cited on page 29)

## BIBLIOGRAPHY

- Mehrfard, A., Fotouhi, J., Taylor, G., Forster, T., Armand, M., Navab, N., and Fuerst, B. (2021). Virtual reality technologies for clinical education: evaluation metrics and comparative analysis. *Computer Methods in Biomechanics and Biomedical Engineering: Imaging & Visualization*, 9(3):233–242. (cited on page 2)
- Minolta, K. (2022). Cs-2000 spectroradiometer. <https://sensing.konicaminolta.us/us/products/cs-2000-spectroradiometer/>. Accessed: 2022-08-02. (cited on pages 31 and 36)
- Morovič, J. (2008). *Color gamut mapping*. John Wiley & Sons. (cited on pages 12 and 15)
- Mulligan, J. B. (2009). Presentation of calibrated images over the web. In *Human Vision and Electronic Imaging XIV*, volume 7240, pages 32–41. SPIE. (cited on pages 3 and 22)
- Niu, M. (2020). Application of intelligent virtual reality technology in clothing virtual wear and color saturation after covid-19 epidemic situation. *Journal of Intelligent & Fuzzy Systems*, 39(6):8943–8951. (cited on page 2)
- Ottosson, B. (2021a). Interactive color picker comparison. <https://bottosson.github.io/misc/colorpicker/>. Accessed: 2022-07-26. (cited on page 16)
- Ottosson, B. (2021b). Two new color spaces for color, picking - okhsv and okhs1. <https://bottosson.github.io/posts/colorpicker/>. Accessed: 2022-07-15. (cited on pages 9 and 15)
- Parraga, C. A., Roca-Vila, J., Karatzas, D., and Wuerger, S. M. (2014). Limitations of visual gamma corrections in lcd displays. *Displays*, 35(5):227–239. (cited on page 41)
- Pascale, D. (2006). Rgb coordinates of the macbeth colorchecker. *The BabelColor Company*, 6. (cited on page 36)
- Pigeon, S. (2022). Hsv and hsl (colorpsaces xi). <https://hbfs.wordpress.com/2018/07/03/hsv-and-hsl-colorpsaces-xi/>. Accessed: 2022-08-05. (cited on page 13)
- Rhyne, T.-M. (2017). Applying color theory to digital media and visualization. In *Proceedings of the 2017 CHI Conference Extended Abstracts on Human Factors in Computing Systems*, pages 1264–1267. (cited on pages 9, 12, 13, 14, and 15)
- Rueda, M.-J. (2022). Open source software for hue judgments collection. <https://github.com/Mariajru>. Accessed: 2022-08-05. (cited on page 4)

## BIBLIOGRAPHY

- Sharma, A. (2018). *Understanding color management*. John Wiley & Sons. (cited on pages 6, 7, 9, 11, 17, 18, 19, 20, and 57)
- Sharma, G. and Bala, R. (2017). *Digital color imaging handbook*. CRC press. (cited on pages 6, 8, 16, 17, 18, and 20)
- Sik Lányi, C. and Schanda, J. (2011). Analysing the colours of the virtual reality museum's picture. *Acta Polytechnica Hungarica*, 8(5):137–150. (cited on page 2)
- Smith, A. R. (1978). Color gamut transform pairs. *ACM Siggraph Computer Graphics*, 12(3):12–19. (cited on page 33)
- Soneira, R. M. (2016). Display color gamuts: Ntsc to rec. 2020. *Information Display*, 32(4):26–31. (cited on page 13)
- To, L., Woods, R. L., Goldstein, R. B., and Peli, E. (2013). Psychophysical contrast calibration. *Vision research*, 90:15–24. (cited on page 41)
- W3C (1996). Png (portable network graphics) specification. <https://www.w3.org/TR/PNG-GammaAppendix.html>. Accessed: 2022-07-26. (cited on page 18)
- W3C (2022). <https://www.w3.org/>. Accessed: 2022-07-21. (cited on page 15)
- Witzel, C. and Gegenfurtner, K. R. (2018). Are red, yellow, green, and blue perceptual categories? *Vision research*, 151:152–163. (cited on page 31)
- Wool, L. E., Komban, S. J., Kremkow, J., Jansen, M., Li, X., Alonso, J.-M., and Zaidi, Q. (2015). Salience of unique hues and implications for color theory. *Journal of vision*, 15(2):10–10. (cited on page 31)
- Wuerger, S. (2008). Colour calibration. US Patent 7,425,965. (cited on pages 2, 37, and 41)
- Xiao, K., Fu, C., Karatzas, D., and Wuerger, S. (2011a). Visual gamma correction for lcd displays. *Displays*, 32(1):17–23. (cited on page 22)
- Xiao, K., Wuerger, S., Fu, C., and Karatzas, D. (2011b). Unique hue data for colour appearance models. part i: Loci of unique hues and hue uniformity. *Color Research & Application*, 36(5):316–323. (cited on pages 24 and 29)

# List of Figures

2.1	Hierarchical steps that define the color management process. . . . .	7
2.2	Calibration and characterization workflow. . . . .	8
2.3	CIE 1931 and CIE 1976 Chromaticity Diagrams. . . . .	10
2.4	Adobe Wide Gamut RGB, DCI-P3, and sRGB gamuts representation in the xy chromaticity diagram. . . . .	12
2.5	Representation of RGB color space. . . . .	13
2.6	HSV and HSL color spaces. . . . .	14
2.7	Visualization of the sRGB irregular shape in the CIELAB color space. .	16
2.8	RGB Primaries in ColorSync Utility. . . . .	17
2.9	Visualization of the gamma value effects. . . . .	19
2.10	Characterization process based on physcal model. . . . .	21
3.1	Stages visualization of the data collection. . . . .	23
3.2	GUI Introduced rotations. . . . .	24
3.3	Experimental workflow for the visual judgments. . . . .	25
3.4	Grey annuli displayed in the neutral grey task. . . . .	26
3.5	Saturation arrangement between consecutive trials. . . . .	27
3.6	Visualization of the new hue angles calculation in the HSV color model. . . . .	28
3.7	Visualization of the red hue plane. . . . .	30
3.8	Selected coordinates to define the hue planes. . . . .	31
3.9	Okhsv implementation visualization. . . . .	32
4.1	Calibration workflow . . . . .	35
4.2	Hue planes visualization in HSV and RGB color models . . . . .	36
4.3	Visualization of the measurement workflow. . . . .	36
4.4	Visualization of the yellow-blue hue plane in the HSV color space. .	37
4.5	Conversions direction. . . . .	39
4.6	Computing and applying the matrix-based transformation. . . . .	40
4.7	Visualization of 3D points fitting into a plane. . . . .	42
4.8	Point-to-Point hue compensation. . . . .	44
5.1	ColorChecker . . . . .	47
5.2	$\Delta E_{00}$ values for the second Conversion, and the Point-to-Plane transformation. . . . .	49
5.3	$\Delta E_{00}$ values for the second Conversion, and the Point-to-Plane transformation. . . . .	50

## LIST OF FIGURES

5.4	$\Delta E_{00}$ values for the first Conversion, and the White preservation transformation. . . . .	50
5.5	$\Delta E_{00}$ values for the second Conversion, and the Point-to-Point transformation. . . . .	52
5.6	$\Delta E_{00}$ values for the second Conversion, and the Point-to-Plane preservation transformation. . . . .	52
5.7	$\Delta E_{00}$ values for the second Conversion, and the White preservation transformation. . . . .	53
5.8	Unique hue selections over the CIE 1976 Chromaticity Diagram . . . . .	54
5.9	Orange hue selections over the CIE 1976 Chromaticity Diagram . . . . .	54
5.10	Hue set $\Delta E_{00}$ comparison . . . . .	55

# List of Tables

2.1	sRGB specifications . . . . .	11
3.1	Selected Saturation-Value combination points to sample a hue plane.	30
4.1	Designed profiles white point and hue specifications. . . . .	38
5.1	Mean and STD of $\Delta E_{00}$ for two conversions. . . . .	51